THE MEASUREMENT OF NUCLEAR GYROMAGNETIC RATIOS OF SHORT LIVED STATES USING INTERNAL FIELDS

Thesis by
James David Bowman

In Partial Fulfillment of the Requirements

For the Degree of
Doctor of Philosophy

California Institute of Technology
Pasadena, California
1968
(Submitted June 28, 1967)

ACKNOWLEDGMENTS

The experiments reported here were carried out in collaboration with Dr. Kumar Bhattacherjee and Mr. Elton Kaufmann. The author wishes to express his appreciation for their cooperation.

The author wishes to thank Prof. Felix Boehm for his guidance and encouragement throughout the author's graduate studies.

The author wishes to thank Drs. Edwin Seltzer and John Trischuck for a number of stimulating discussions, and Mr. Herbert Henrikson whose skill in the design of experimental apparatus has been invaluable.

This work was supported in part by the United States Atomic Energy Commission.

ABSTRACT

The nuclear gyromagnetic ratios of the first excited 2^+ states in ^{114}Cd, ^{122}Te and ^{124}Te have been measured to be $.42 \pm .06$, $.31 \pm .03$ and $.22 \pm .05$ μ_N respectively. The perturbed gamma-gamma angular correlation method was used. The large experimentally known hyperfine fields present at the positions of the nuclei of substitutional impurity atoms in an iron lattice were used to obtain mean angles of precession large enough to be measured. The experimental results are compared with theory, and with the results of Coulomb excitation implantation measurements. In each instance the agreement is poor.

TABLE OF CONTENTS

I. INTRODUCTION

The gyromagnetic ratio or g factor of a nuclear state is defined as the ratio of its magnetic dipole moment to its angular momentum measured in units of $\hbar$ and is given in units of nuclear magnetons. The determination of the g factors of excited states of nuclei provides a test for our understanding of nuclear structure. Our meager knowledge of g factors and static electric quadrupole moments in the vibrational region is in marked contrast to the extensive data that are available for rotational nuclei. The low-lying excited states of rotational nuclei have been intensively investigated by the Mössbauer and perturbed angular correlation techniques. The high energies and short lifetimes of the first excited states of even - even vibrational nuclei make their study by the Mössbauer technique impossible.

Until recently perturbed angular correlation measurements have also been impractical because of the short lifetimes of vibrational states, which are typically 10^{-11} seconds. In order to measure the g factor of a state having such a lifetime, it is necessary to have a magnetic field of the order of 500 kilogauss. Although such magnetic fields cannot be produced statically on a macroscopic scale, it has been found that hyperfine fields of this magnitude are present at the location of the nuclei of impurity atoms in ferromagnetic hosts.[1] We have utilized this method of the "internal fields" in the measurement of the g factors of the first excited 2^+ states in ^{114}Cd, ^{122}Te, and ^{124}Te. These states were populated by the radioactive decays of $^{114}In^m$, ^{122}Sb, and ^{124}Sb respectively.

To obtain a semi-classical estimate for the nuclear g factor of a collective state one considers the nucleus as a fluid undergoing irrotational flow. This "hydrodynamic" estimate gives the value Z/A, where Z is the charge number and A the nucleon number. More elaborate theoretical descriptions of first excited states of vibrational nuclei, based on both a collective and a microscopic description of the nuclear motion, predict from twice to half this value.[2][3] In the case of tin isotopes even negative g factors are predicted[2] for the first 2^+ state. Obviously, experimental data are needed to help decide which theoretical approach gives an account of the g factors of vibrational states.

The present thesis thus is aimed at providing a test of the theoretical understanding of these states.

A comparison of the results of this thesis with work based on a method using Coulomb excitation is attempted for Te nuclei. The experimental results from Coulomb excitation show a striking increase of the first excited state g factors with neutron number[4]. Our experiments on ^{122}Te and ^{124}Te disagree with these findings. A possible reason for this disagreement will be discussed.

Thus, the purposes of the work presented here are threefold. They are, to obtain information relevant to the theoretical understanding of vibrational nuclei, to explore and develop the possibilities of the utilization of hyperfine magnetic fields present at the nuclei of impurity atoms dissolved in ferromagnetic hosts, and to obtain an independent check on previous work done by the Coulomb excitation method.

II. DESCRIPTION OF THE EXPERIMENTAL METHOD

2.1 Introduction

In 1950 Brady and Deutsch[5] pointed out the possibility of using the anisotropic angular correlations in γ-ray cascades to measure the g factors of excited nuclear states. The first such measurement was carried out in 1951[6]. Since the formalism needed to interpret our experimental results has been treated in several excellent articles[7] we will give here only a brief description of the method.

2.2 Angular Correlations

Figure 1 shows an idealized γ-γ cascade. The first radiation, called γ_1, leads to a non-uniform population of the magnetic sub-levels of the intermediate state. The second radiation γ_2 will then exhibit a non-isotropic pattern of emission with respect to the direction of emission of γ_1. The probability distribution for the emission of the two γ quanta depends on θ, the angle between their directions of propagation, and can be expressed as:

$$W(\theta) = \sum_{k,\,\text{even}}^{k_{max}} A_{kk}\, P_k(\cos(\theta)) \qquad (1)$$

where the A_{kk} depend on the multipolarities of the radiations and on the spins and parities of the three levels. Among the selection rules for the value of the largest index present in the above sum is

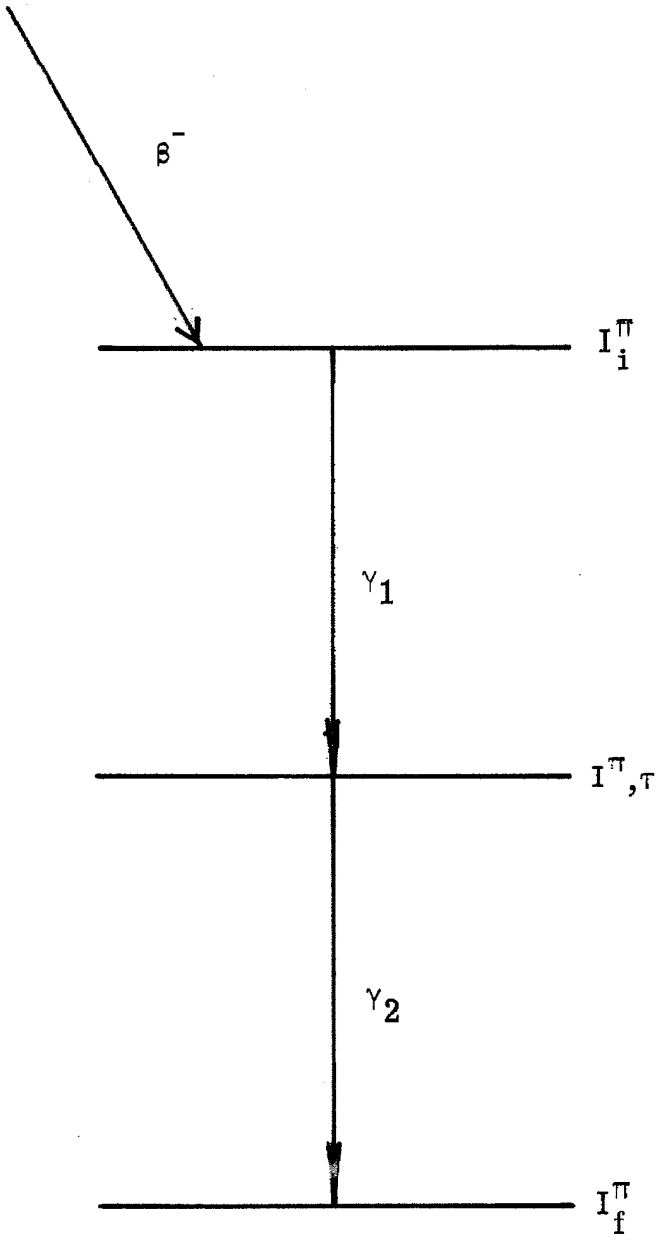

Figure 1. Showing typical γ-γ cascade, in this case the highest excited state is populated by β decay. I_i^π, I^π and I_f^π are the spins and parities of the initial or highest, the intermediate, and the final excited states respectively. The mean life of the intermediate state is τ.

the relation

$$k_{max} \leq 2I \tag{2}$$

where I is the angular momentum of the intermediate state. Since our experiments involve states of angular momentum two, it is possible to limit the sum to the first three terms.

2.3 Angular Correlations Perturbed by a Magnetic Field

If one applies a magnetic field to a nucleus, then it will precess about the direction of the applied field with a Larmor frequency $\omega_L = - g\mu_N H/\hbar$. Here g is the g factor of the excited state, μ_N is the nuclear magneton, and H is the magnetic field strength. If the direction of the applied field is perpendicular to the plane of the directions of emission of the γ rays, then formula (1) is modified in the following way:

$$W(\theta, H, t) = \sum_{k, \text{even}}^{k_{max}} A_{kk} P_k(\cos(\theta - \omega_L t)) \tag{3}$$

where t is the time that the nucleus spends in the excited state, and $\omega_L t$ is just the angle of rotation that the nucleus experiences while in the intermediate state. If the angle of rotation which the nucleus experiences during the lifetime of the intermediate state is small i.e., $\omega\tau << 1$ and t is not measured, then formula (3) yields upon expanding and averaging over the lifetime of the state

$$\overline{W}(\theta, H) = \sum_{k,\,\text{even}}^{k_{max}} A_{kk}\left(P_k(\cos(\theta)) - \frac{\partial P_k(\cos(\theta))}{\partial \theta}\,\omega_L\tau\right)$$

$$= W(\theta) - \frac{\partial W(\theta)}{\partial \theta}\,\omega_L\tau \ . \qquad (4)$$

Our experiments consisted of the measurement of $W(\theta)$ and $\overline{W}(\theta, H)$. Scintillation spectrometers were used to detect γ_1, and γ_2. The arrangement of the source and detectors is shown in figure 2. The coincidence counting rate for an angle θ between the two detectors is proportional to $W(\theta)$ when no fields act upon the nucleus while it is in the intermediate state. If a magnetic field is applied to the source, as shown in figure 2, then the coincidence counting rate will change according to formula (4).

This effect was utilized for the measurement of the mean angle of rotation $\omega_L\tau$. Since

$$\omega_L\tau = -\frac{g\mu_N H\tau}{\hbar}\ , \qquad (5a)$$

or numerically,

$$\omega\tau(\text{Radians}) = -\frac{g \times H(\text{kilogauss}) \times \tau(\text{nanoseconds})}{209.1}\ , \qquad (5b)$$

if H and τ are known, and $\omega_L\tau$ is measured then g can be deduced.

The A_{kk} which are experimentally determined will not be those given in formula (3). They will be modified according to the

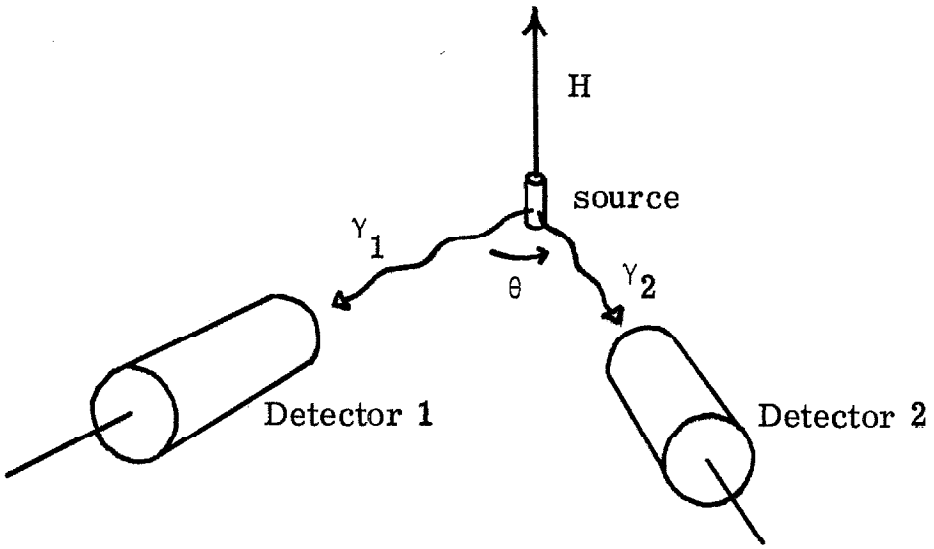

Figure 2. Showing the arrangement of source, detectors and the magnetic field H.

relation (6)

$$A_{kk}^{exp} = G_k^1 G_k^2 A_{kk} , \qquad (6)$$

where the G_k^1 and G_k^2 depend upon the geometries of detectors one and two, which in practice subtend a finite solid angle, while formula (1) assumes an infinitesimally small angle of acceptance. The factors G_k^1 and G_k^2 do not enter into the determination of $\omega_L \tau$ since $W(\theta)$ and $\overline{W}(\theta, H)$ are measured in the same geometrical configuration.

2.4 Necessity for the Use of Internal Fields

In order that in a precession experiment the second term on the right side of equation (5a) be measurable with sufficient accuracy, it is necessary that $\omega_L \tau$ be at least of the order of .01. The lifetime of vibrational states is typically 10^{-11} seconds; thus if we assume $g \approx Z/A \approx .4$ we need a magnetic field of H = 500 kilogauss. A static laboratory field this large is unobtainable using presently available techniques.

In 1959 Samoilov, et al.[8] demonstrated the existence of large hyperfine fields at the nucleus of a diamagnetic impurity atom introduced in dilute form into an iron lattice. They employed the nuclear orientation technique and found a field of 250 kilogauss for indium dissolved in iron. Since then considerable experimental information on the systematic variation of these fields with the Z of the impurity atom has been accumulated using perturbed angular

correlation, nuclear magnetic resonance, nuclear orientation and Mössbauer techniques. An up to date compilation of the measured values of the internal fields for the elements Ru, Rh, Pd, Ag, Cd, In, Sn, Sb, Te, I, and Xe is given in figure 3[1][9][10]. The origin of these fields can be accounted for qualitatively on the basis of the effects of the polarization of conduction electrons and core electrons which produce a magnetic field at the nucleus via a Fermi contact term[11]. A quantitative understanding, however, is still lacking. Nevertheless, our empirical knowledge of the fields is quite good, and hence they are useable in experiments to measure nuclear magnetic moments.

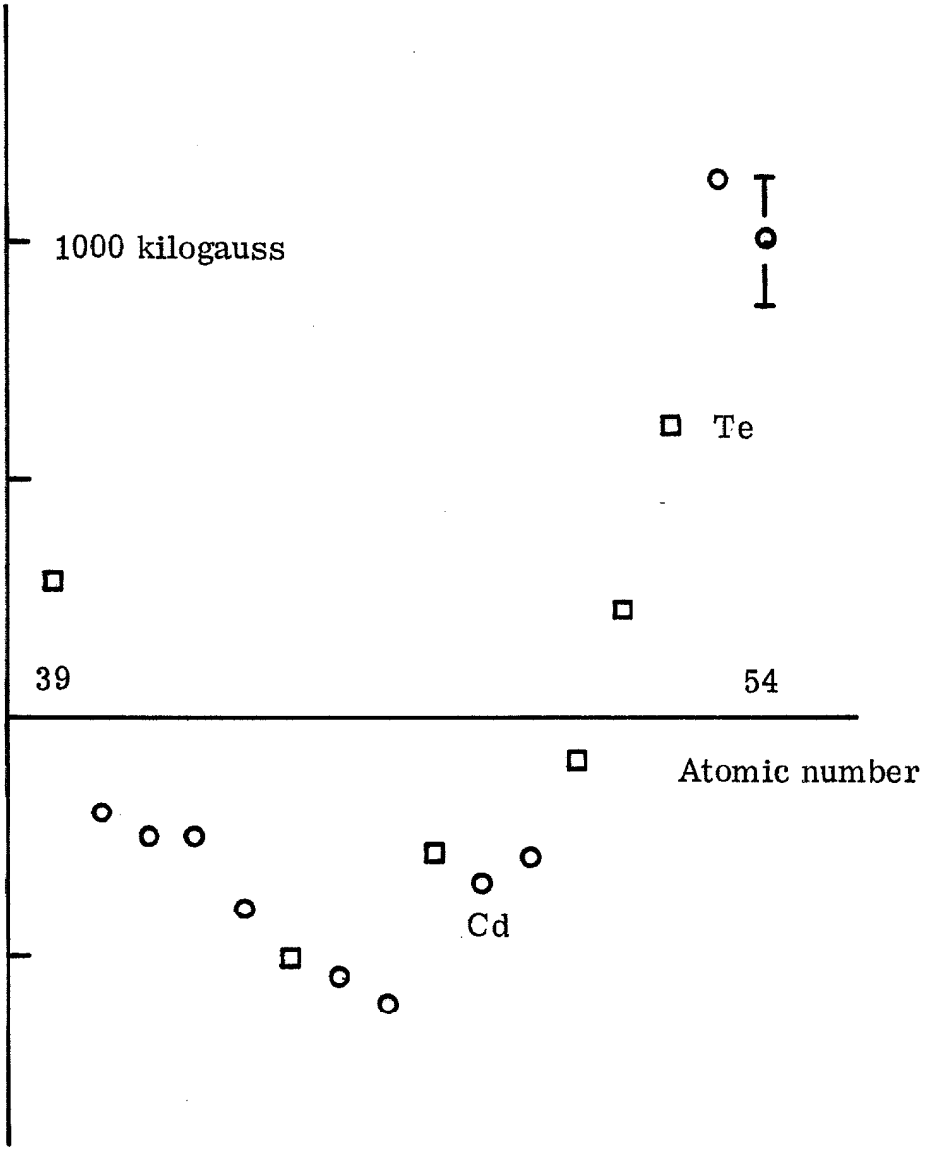

Figure 3. Showing the variation of the internal hyperfine field in iron as a function of the atomic number of the impurity. In most cases, the error bars are too small to be shown. Square points indicate that the sign of the hyperfine field is known as well as its magnitude. For the circles only the magnitude is known.

III. POSSIBLE SOURCE OF SYSTEMATIC ERRORS IN THE MEASUREMENT OF $\omega\tau$

3.1 Introduction

It has been assumed that the only field acting upon the nucleus while it is in the intermediate state is the internal hyperfine field. The presence of other fields, electric field gradients or magnetic fields other than the hyperfine field, would complicate the interpretation of our results. The excited state under study is always the intermediate state of γ-γ cascade. The γ ray that populates the state under study, or preceding radiations may impart a momentum to the atom sufficient to eject it from its lattice position. That is, the lattice may be locally radiation damaged. The preceding radiations may leave the atom in an ionized state, or in some highly excited state. In the time before the atom decays to its ground state the nucleus will be subject to an internal field which will be different from that which we assume. The influence of these effects on our measurements is discussed in this section.

3.2 Fields Due to Lattice Imperfections

The body centered cubic structure of α iron has cubic symmetry about each lattice site, so the electric field gradient must vanish for substitutional impurity atoms. Hence, the only other fields present will be those due to lattice imperfections. The very short excited state lifetimes are of advantage in this respect. Unless residual electric field gradients or magnetic fields are very

strong indeed they will produce a negligible reorientation of the nucleus during the lifetime of the excited state. If these fields are assumed to be randomly oriented, then their perturbation of the angular correlation will be proportional to $(\omega_R \tau)^2$ where ω_R is some measure of the strength of the residual field and τ is the nuclear lifetime. Magnetic and quadrupole interaction frequencies are typically 10^8-10^9 Hertz[12]. For $\omega_R = 10^9$ we obtain $(\omega_R \tau)^2 = 10^{-4}$, assuming $\tau = 10^{-11}$ seconds.

Kontani and Itoh[13] have found non-unique internal fields in alloys having impurity concentrations of the order of one percent. They attribute these non-unique fields to the interaction of impurity atoms. The impurity concentration of our samples was typically 10^{-2} percent, hence such effects are assumed to be unimportant for our measurements.

3.3 Local Radiation Damage

In all cases our experiments involve radiations with energies of the order of 1 MeV. The energy imparted to a Te^{124} nucleus by the emission of a 1 MeV γ ray is about 4 eV. The threshold energy for the production of a lattice defect consisting of a hole interstitial pair, a Frenkel defect, in pure iron has been determined to be 22 eV[14]. No such data are available for the Cd-Fe system, or the Te-Fe system: however, it can be argued that somewhat more energy is required to eject a telurium or cadmium impurity from its lattice position. The threshold energy is the sum of two parts: the binding energy of an atom in the lattice and the energy associated with an atom in an interstitial location. The boiling point of iron, 3000 C^o,

corresponds to an energy of an iron atom in an iron lattice of about 1/3 eV, which is negligible compared to 22 eV. Thus, one may conclude that most of the threshold energy for the displacement of an atom from a sustitutional to an interstitial location is associated with the creation of the interstitial. The atomic radii of telurium and cadmium are larger than that of iron: 1.60, 1.51 and 1.26×10^{-8} cm. respectively; hence, the energy associated with putting a telurium or cadmium atom in an interstitial location is probably larger than the corresponding energy for iron, and hence the threshold energy for the displacement of a substituted telurium or cadmium atom into an interstitial location is greater than that for the creation of a Frenkel pair in an iron lattice.

In the case of Te^{124} two indcpendent measurements of $\omega\tau$ were performed in which the radiations populating the states had energies of .722 and 1.69 MeV. This corresponds to energies of 2.2 and 11.7 eV imparted to the Te atom. If the effect under discussion were important, one would expect it to show up as a difference in the values of $\omega\tau$ measured in these two experiments. We find, however, that the two results are in excellent agreement, although the error of the 1.69 MeV experiment is 40 percent.

3.4 Effect of Preceding Radiations on the Internal Field

The radioactive decay that populates the highest excited state involved in the γ-γ cascade may leave the atomic electrons in an excited state. In the case of ^{114}Cd this highest excited state is populated by K capture, which leaves a K hole in the atomic clectrons. The highest excited states in ^{122}Te and ^{124}Tc arc

populated by β decay which changes the nuclear charge and hence may leave the electrons of the daughter atom in excited states.

The magnetic fields that we assume in the analysis of our data have been measured using the Mössbauer effect in the Te^{125} 35 keV first excited state, mean life 2.0 ± .3 nanoseconds[9], and by perturbed angular correlation measurements involving the 247 keV level in Cd^{111}, mean life 122.5 ± .7 nanoseconds.[15] These internal fields result from the ground state electronic configuration; hence, they will be applicable only if the electronic disturbances caused by preceding radiations have "healed out" before the nucleus decays to the state whose g factor is being measured. It is thus necessary to compare the lifetimes of the highest excited nuclear state involved in the γ-γ cascade to the time required for the atomic electrons to reach their ground state.

The lifetimes of this highest excited state are 2.0 ps. for ^{114}Cd[16], 1.0 ps for ^{122}Te[7], .60 ps for the 1.326 MeV state in ^{122}Te (assuming that B(E2, 2 → 2) is the same as in ^{122}Te), and 6×10^{-17} s for the 2.295 MeV level in ^{124}Te (assuming that the 1.69 MeV γ is E1 and B(E1, 3 → 2) is one single particle unit). Electronic disturbances in the K shell have lifetimes of the order of 10^{-15} - 10^{-17} seconds: the decay mode is principally the emission of X rays, and the lifetimes are determined by line width measurement. Disturbances in intermediate shells decay principally through the Auger effect. The time for an electron hole to move to the outermost shell has been calculated to be 10^{-14} seconds for argon and 10^{-15} seconds for gold.[18] A hole in the outermost shell will be filled in a time comparable to the relaxation time for a classical charge distribution, 10^{-14} seconds for iron.

Hence, the total time for the "healing out" of electronic disturbances is of the order of 10^{-14} seconds. This time is short compared to the first three lifetimes quoted above, but long compared to the lifetime of the 2.295 MeV state in ^{124}Te. Thus, we are safe in assuming the static fields to be appropriate to the measurements involving the first three states, and we would expect any time dependent field effects to show up as a difference between the two $\omega\tau$ measurements in ^{124}Te. In fact, the two results are in excellent agreement, as was pointed out earlier.

IV. EXPERIMENTAL PROCEDURE AND APPARATUS

4.1 Introduction

Each measurement of the g factor of an excited state consisted of the following steps: (1) Preparation of one or several sources of a dilute alloy of the activity to be studied with iron, (2) Measurement of the angular correlation between γ rays populating and depopulating the excited state; and (3) Measurement of the change in coincidence counting rate of these γ rays upon the reversal of an external magnetic field aligning the magnetization vectors of the domains of the alloy sample. This measurement was performed in geometry identical to that of step (2); in this way, the finite size of the detectors and source and scattering did not affect the values of the observed rotations.

The change in coincidence counting rate is defined as

$$\frac{U - D}{U + D} = R(\theta) \tag{7}$$

where U and D are the coincidence counting rates with the external aligning field up and down respectively. The ratio $R(\theta)$ is related to the mean angle of rotation $\omega_L\tau$ through the equation

$$\omega_L\tau = R \times \left(\frac{\partial W(\theta)}{\partial \theta} / W(\theta)\right)^{-1} \tag{8}$$

assuming $\omega_L \tau \ll 1$. The g factor is then related to $\omega_L \tau$ by the formula

$$g = -\frac{\hbar(\omega_L \tau)}{\mu_N H_{int} \tau} , \tag{9a}$$

or numerically,

$$g = -\frac{209.1\ \omega_L \tau(\text{radians})}{H_{int}(\text{kilogauss})\ \tau(\text{nanoseconds})} . \tag{9b}$$

4.2 Source Preparation

Our sources were prepared by alloying the parent activity with iron. The alloys were prepared by melting the parent activity and very pure iron in an induction furnace. The source preparation technique was designed to satisfy the following requirements: (1) the alloys should be as dilute as possible to avoid the effects of interaction between impurity atoms, (2) no contamination should be introduced in melting process, (3) the melting procedure should be efficient, a large fraction of the activity should not be lost. This was a particularly serious problem in the case of ^{114}Cd because of the low boiling temperature of indium.

In order to satisfy requirement (1), the alloys were made using high specific activities. In all cases, suitable source strengths were obtained using impurity concentrations of .0001 or less than 10^{-2} atomic percent. Typical strengths were 2×10^6 γ

rays with energies above 300 kilovolts per second, into 4π solid angle.

In order to avoid contaminating the samples, they were melted in an argon atmosphere in an induction furnace. A novel flux concentrating device was employed which levitated the molten alloy. As shown in figure 4, the surface in contact with the molten alloy is silver which is virtually insoluble in iron. A thin layer of iron was deposited on the silver boat during the melting process, but the silver was not observed to be affected in any other way.

The efficiency requirement was met by enclosing the activity in a container of pure iron (.99999) before melting. Iron pots with tapered holes and tapered pins were fabricated according to figure 5. The activity was deposited in the pot and the pins driven in under vacuum. The sealed pot was then melted in the flux concentrator. No more than half the activity placed in the pot was lost in the melting procedure.

The samples were forged into rough cylinders, and then coined into the form of right circular cylinders 5 mm. in diameter and 6 mm. in height. If a sample was to be annealed it was washed in nitric acid and then sealed into an evacuated (10^{-5} mm. Hg) quartz tube and heated to the appropriate temperature in a resistance heating furnace. No measurable activity was lost in the annealing process.

4.3 Apparatus

The apparatus consisted of: the detectors, the magnet and the electronics.

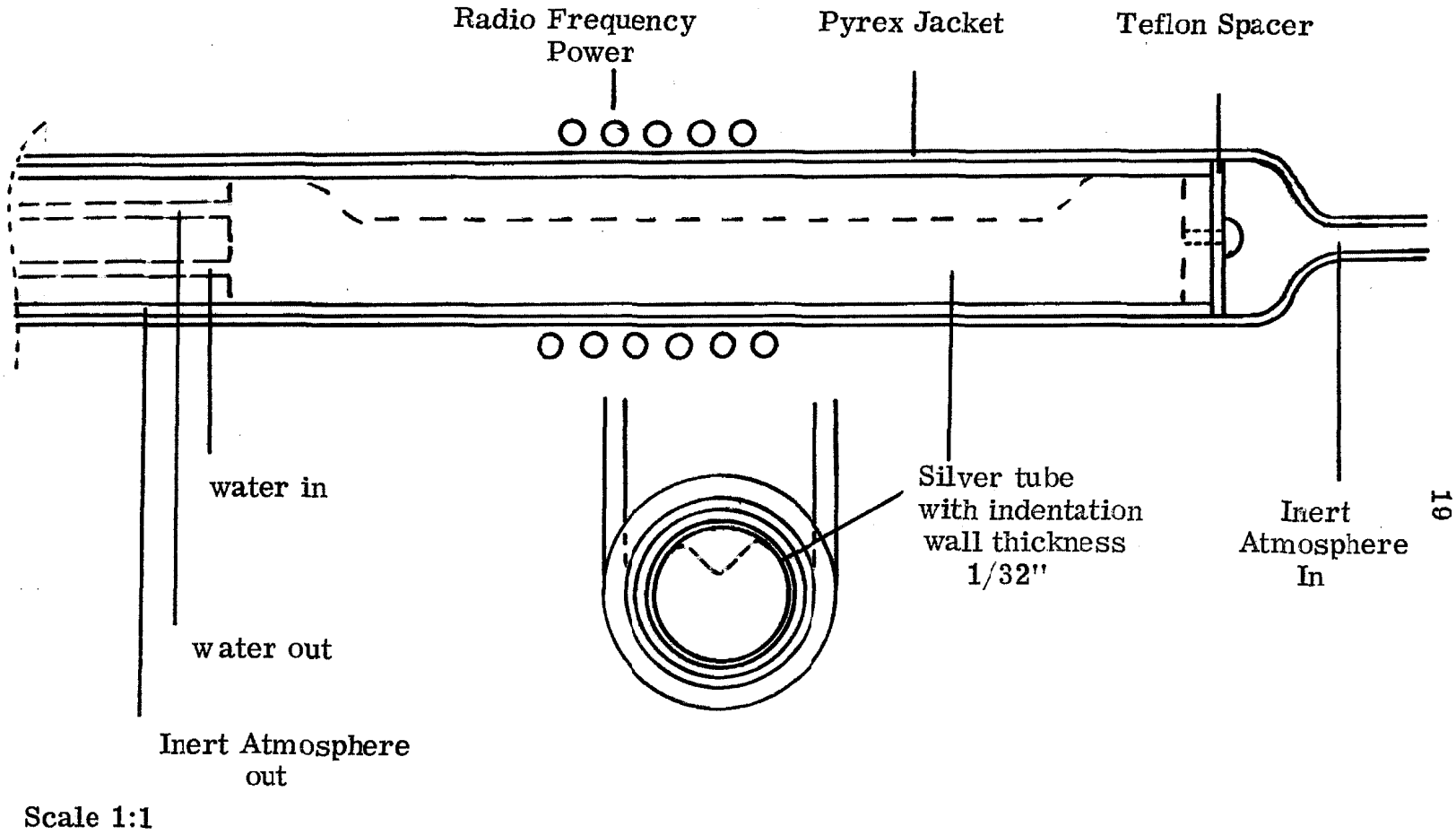

Figure 4. Silver Boat Used in Preparing Alloy Samples.

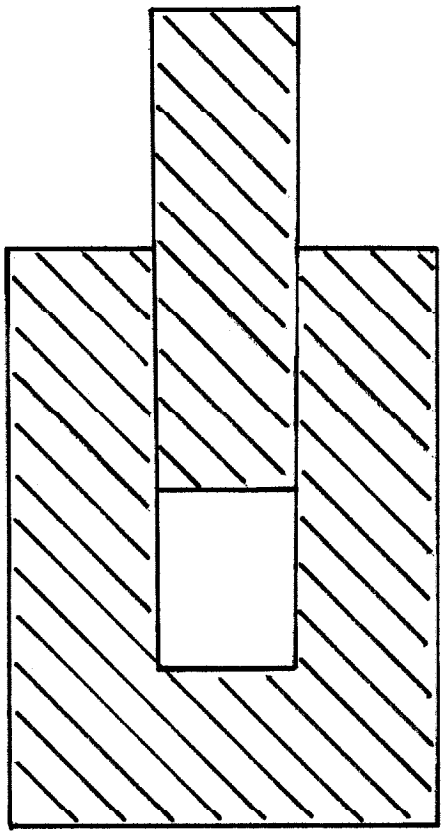

Scale 10:1

Figure 5. Showing tapered pin and pot. The taper is 1/50. When the pin is driven in, there is one .001 inch of interference.

The γ rays were detected in 3" thick x 1 1/2" diameter thallium activated sodium iodide crystals. The crystals were optically coupled to 56 A. V. P. photo-multipliers. The photo-multipliers were magnetically shielded with several layers of co-netic and netic foil. Lead absorbers .050" thick were used to eliminate X rays and low energy γ rays. The resolution of the crystal multiplier combinations used was approximately 9 percent for the 661 keV line from ^{137}Cs. A diagram of the crystals and photomultipliers and their shielding from magnetic fields and extraneous radiation is shown in figure 6.

The iron alloy sample was magnetized by a small magnet. The requirements of the magnet design were: saturation of the source sample within the gap, very small fringing field due to the extreme sensitivity of the gain of the photomultiplier tubes to magnetic fields, and small absorption or scattering of γ rays of energy 500 keV or greater.

Figure 7 gives a diagram of the magnet used in the experiments. It is of the toroidal -H type. Saturation of the sample was determined by observing the flux change through the sensing loop shown in figure 7 upon reversing the current direction. A ballistic galvanometer was used for this test. The sample was pure iron which had been formed identically to the source samples and not annealed. Thus, it was expected to have a permeability as low as that of the least permeable source sample. Figure 8 indicates the saturation of this test sample, and shows the working current for the rest of the measurements.

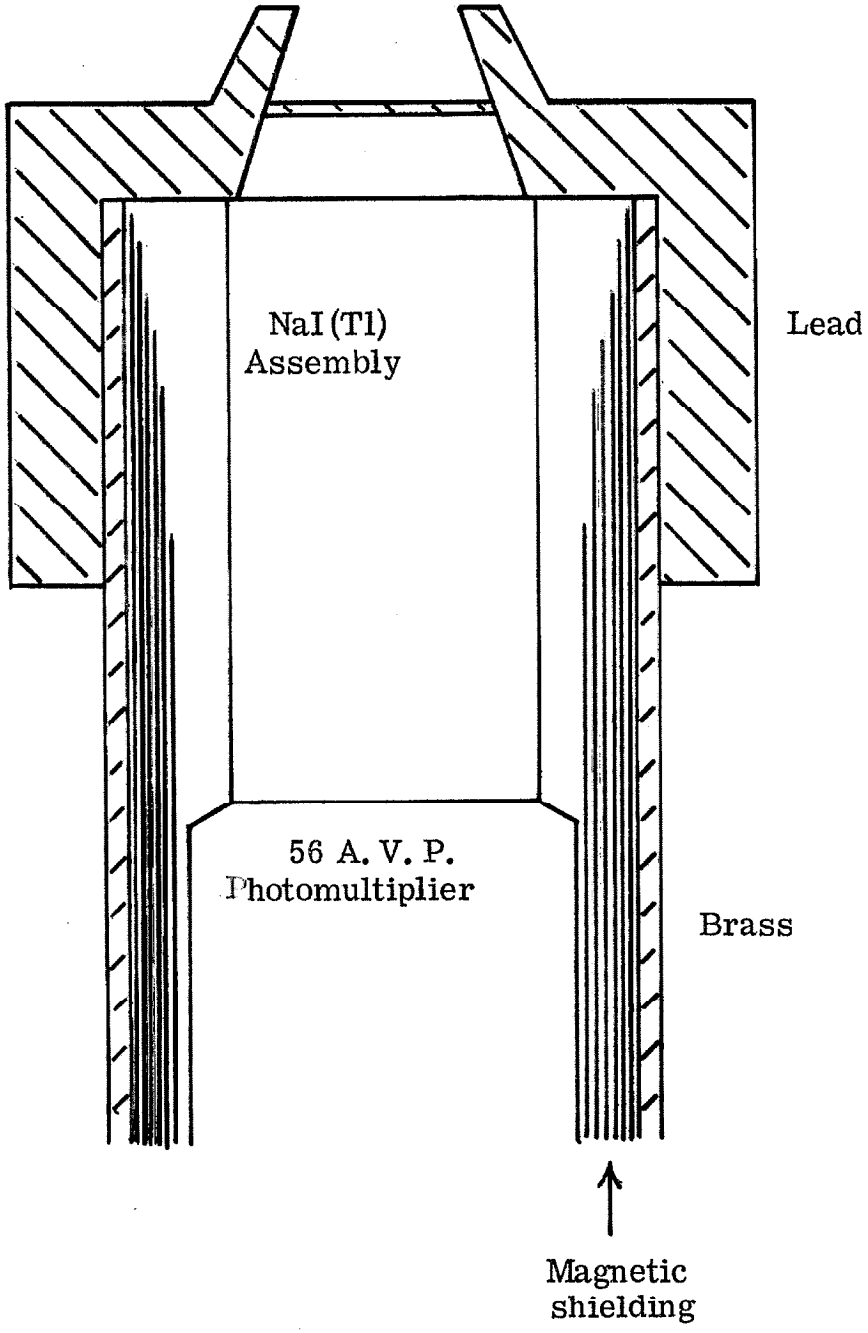

Scale 1:1

Figure 6. Showing detector assembly.

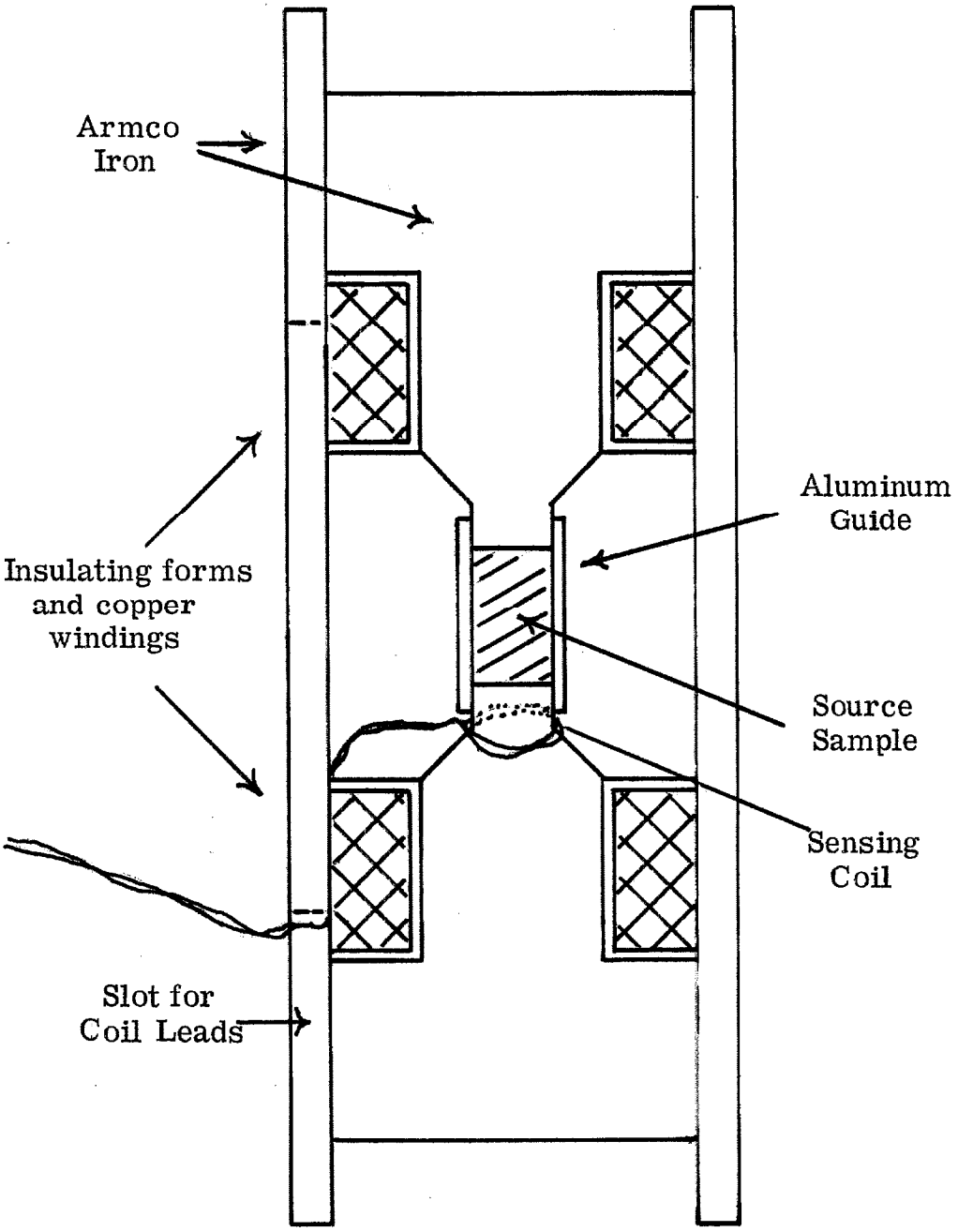

Scale 2:1

Figure 7. Magnet assembly showing sensing coil, and source sample.

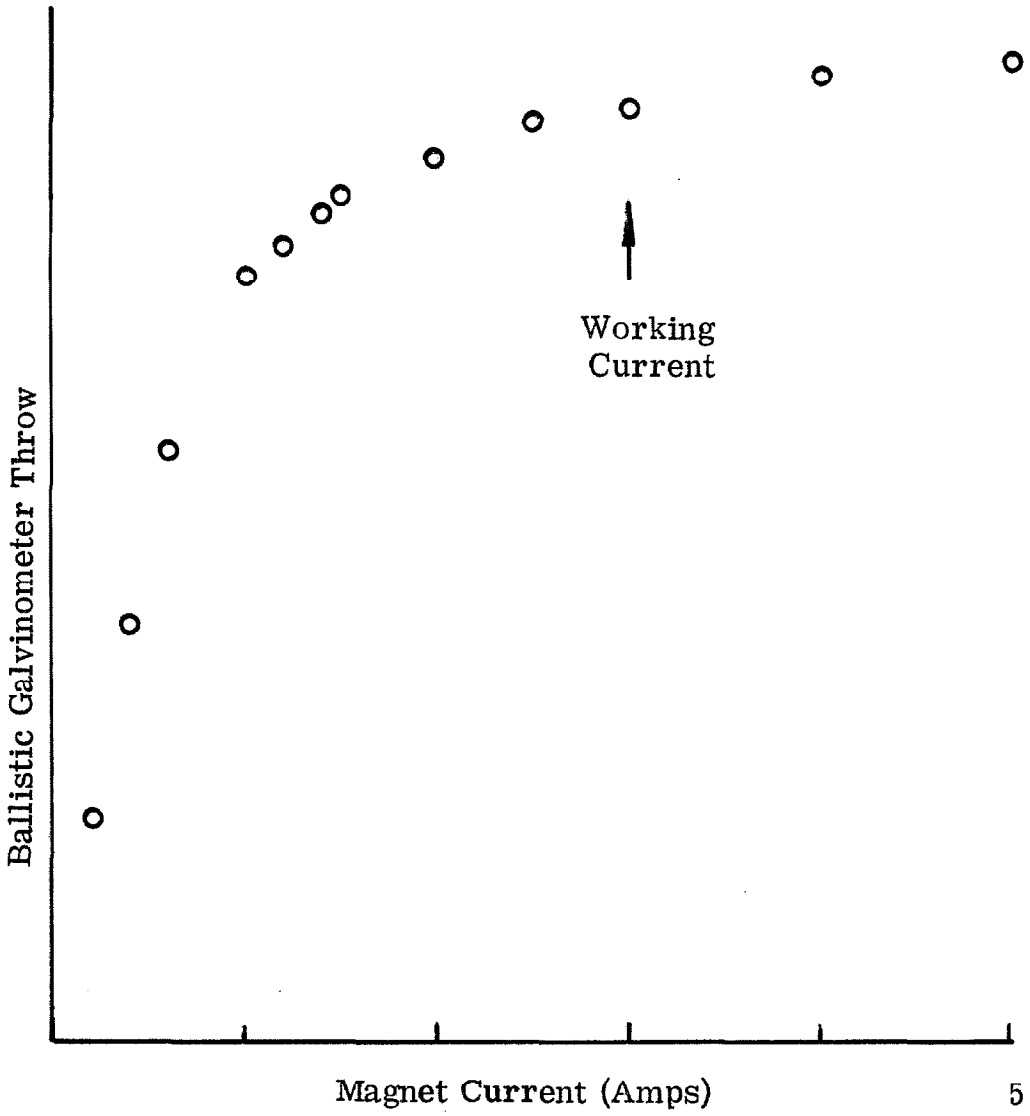

Figure 8. Magnetization of source sample as a function of magnet current.

The magnet had an extremely small fringing field. At the working current this field was less than .1 gauss in the volume occupied by the photomultipliers. The stray field was reduced to less than .005 gauss in the volume of the photomultipliers by adjusting the current through a compensating coil wound around the equatorial plane of the magnet. This current was reversed at the same time as the magnet current. The stray magnetic field was found to have a negligible effect on the gain of the photomultipliers. The fractional change in singles counting rate in each of the detectors was less than 10^{-4} upon the reversal of the aligning field direction.

Angular correlations measured with and without the magnet in place showed that for γ rays with energies above 500 kilovolts, the magnet did not significantly attenuate the magnitude of the angular correlation coefficients.

The photomultiplier pulses were processed by an electronic coincidence system. The change in coincidence counting rate upon the reversal of the magnetic field was small in every case. It was of the order of 2×10^{-3}. Thus, the electronics were designed with the following considerations in mind: ability to accept high counting rates, stability, and good time resolution.

Figures 9abcd give a block diagram of the electronics. This type of coincidence system is called a "slow-fast" system. Two signals were taken from each photomultiplier tube; a linear signal from the 9^{th} dynode, where the pulse height is proportional to the number of electrons emitted from the photocathode, and an anode signal for fast timing purpose.

The current pulse at the anode consists of the sum of many pulses corresponding to the emission of single electrons at the photocathode. These single electron pulses have a width of about 3 ns.

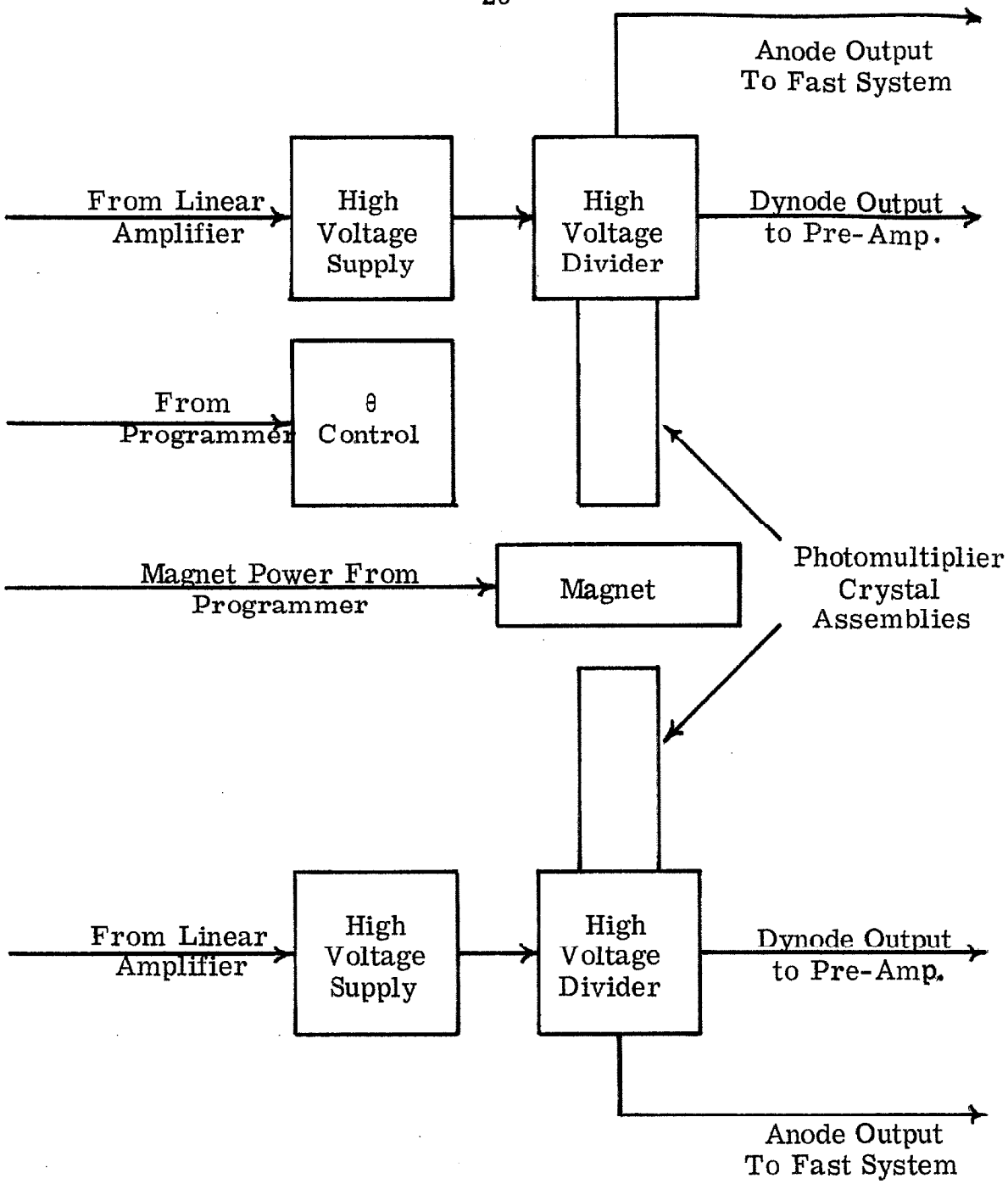

Figure 9a. Detectors and associated apparatus.

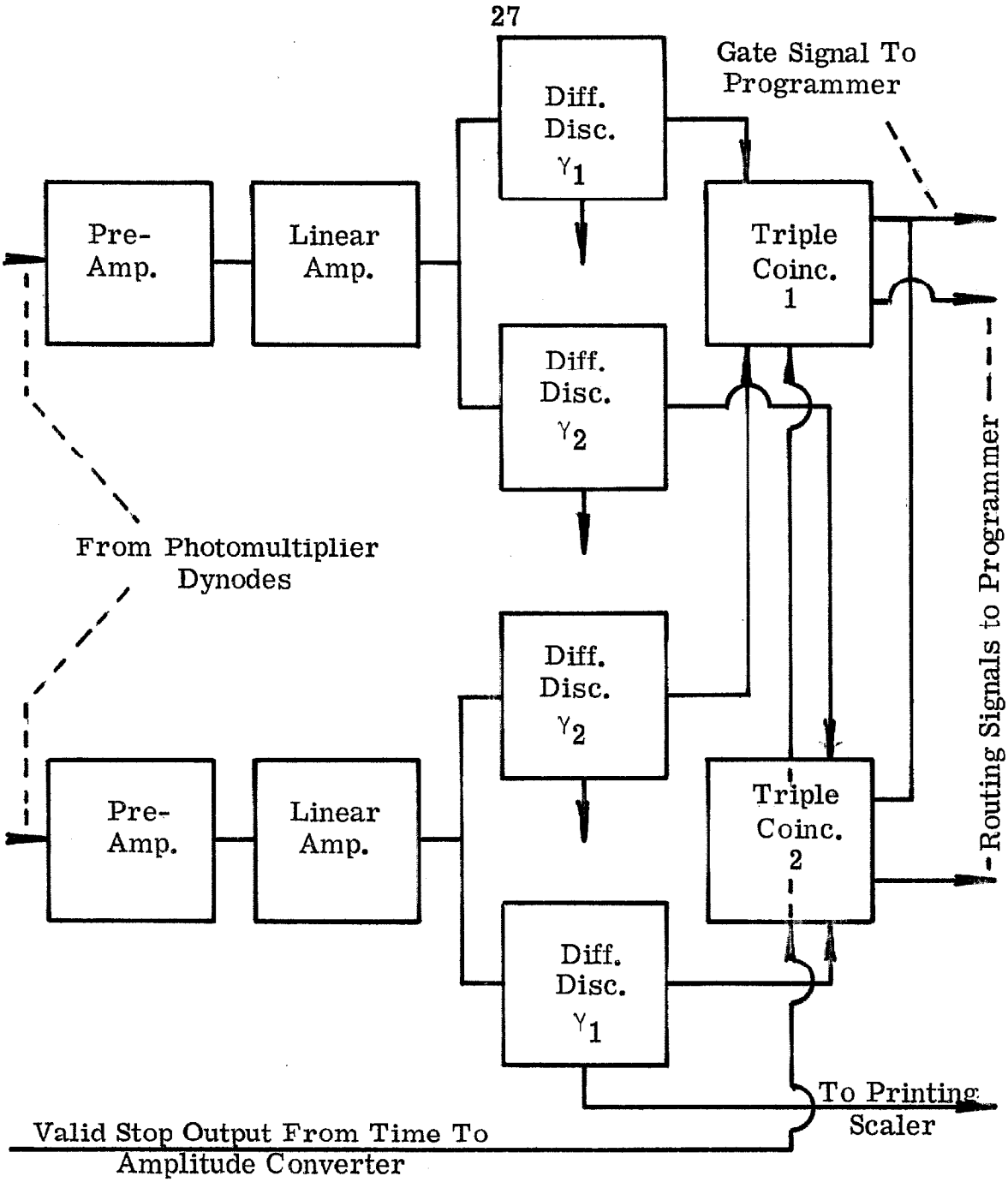

Figure 9b. Linear pulse analysis or slow system. Typical time constants in this part of the electronics are 1 μs. Several interface units have been omitted from the block diagram.

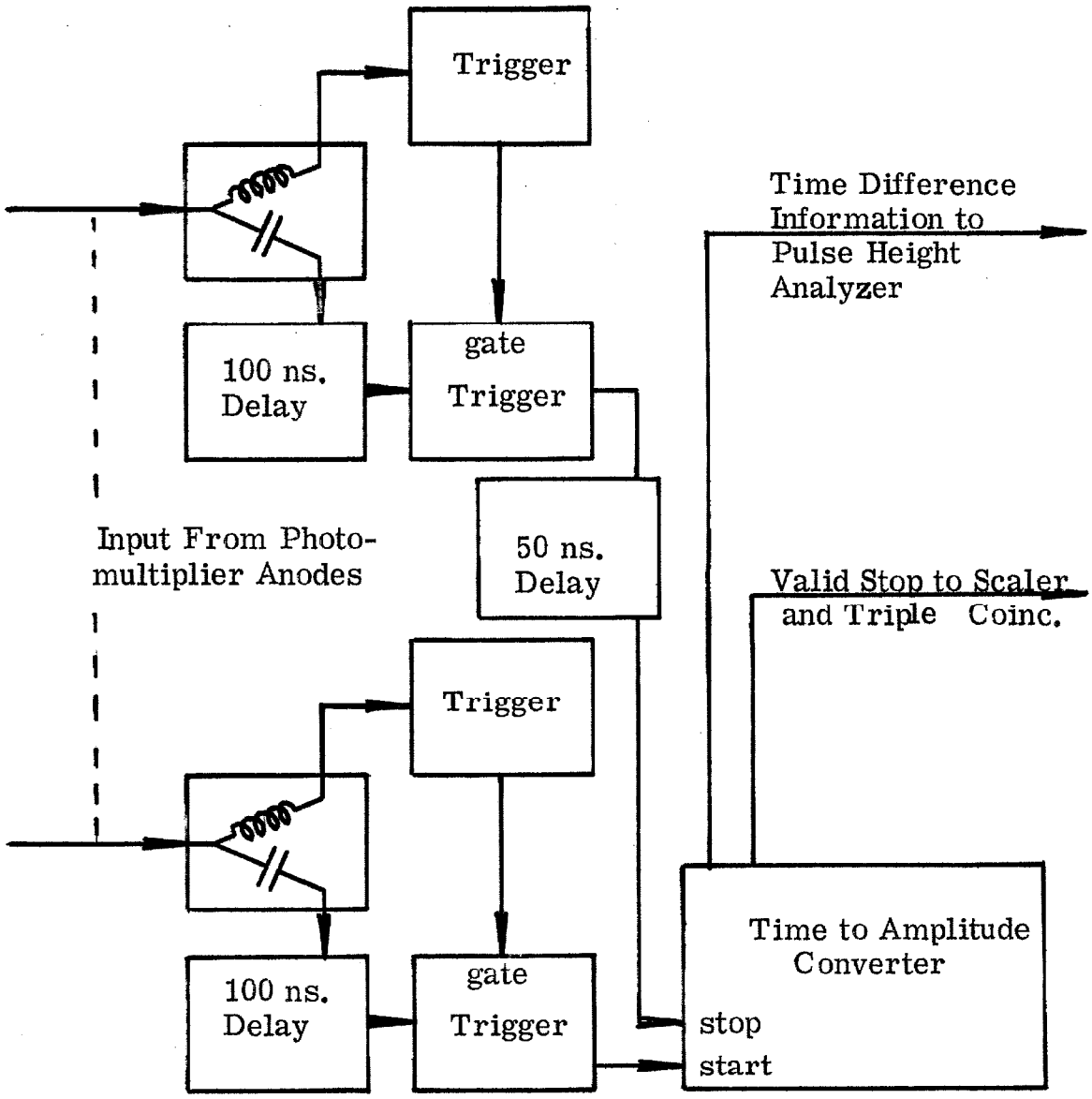

Figure 9c. Fast system, pulse standardization and time to amplitude converter. Typical rise times for pulses in this section of the electronics are 2 ns.

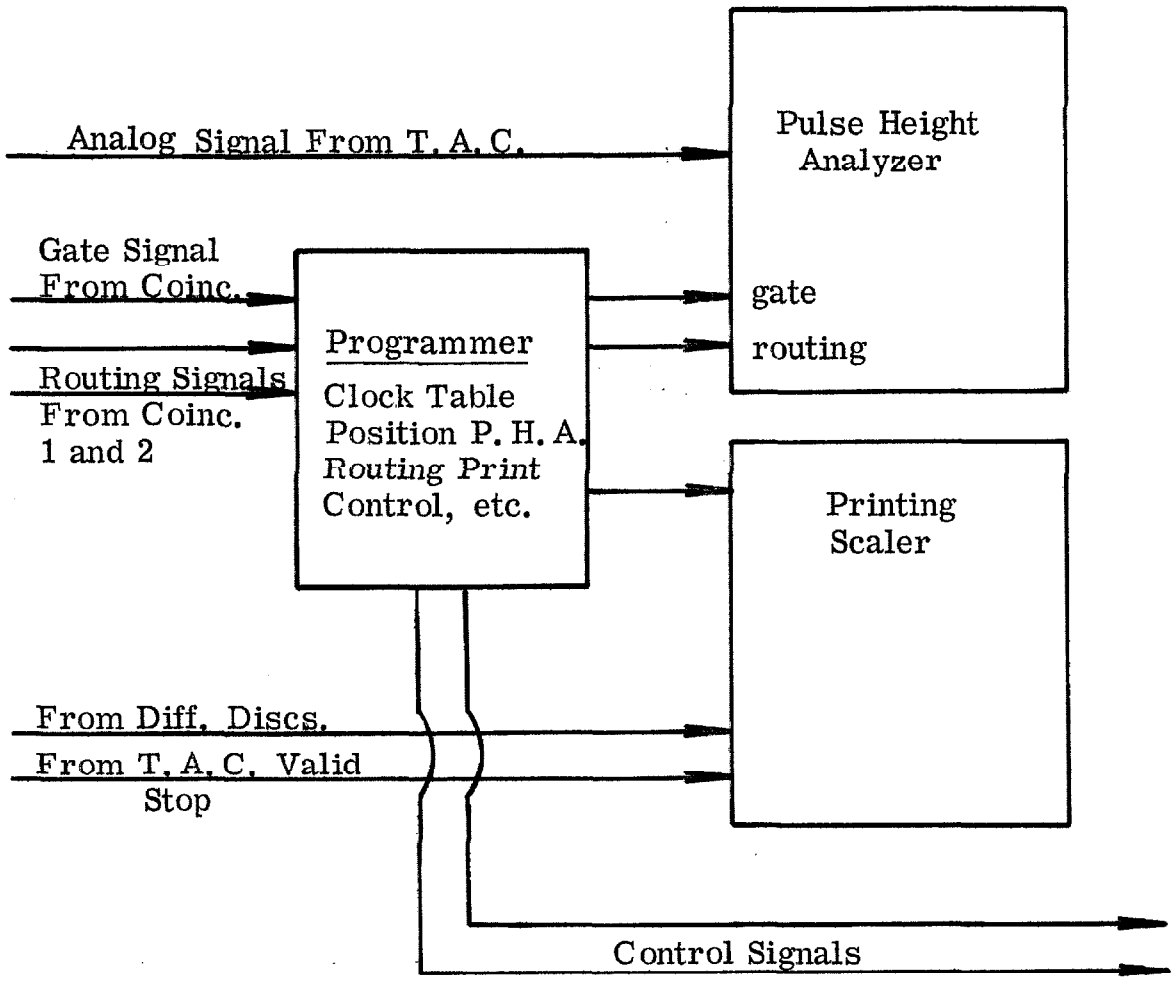

Figure 9d. Control Logic and Data Storage.

for the 56 A.V.P. phototube. It can be shown that in order to obtain the best time resolution the pulse standardization trigger should be sensitive to the pulse corresponding to the emission of the first photo electron from the photocathode.

This trigger level requirement is inconsistent with the use of strong sources, since in order to avoid multiple triggering it would be necessary to use a trigger with a long dead time. The decay time of NaI (Tl) is 250 ns. For a 1 MeV γ ray totally absorbed in the crystal approximately 10^3 electrons will be emitted from the photocathode. The median time for the emission of the last photoelectron from the photocathode would be about 2 μs. after the 1 MeV γ ray impinged on the crystal. Thus, with a dead time of 2 μs. 50 percent of such pulses would double trigger.

In order to avoid this difficulty the anode pulse was split into a high and a low frequency component by an LC network as shown in figure 9c. A low level trigger accepting the delayed high frequency component was gated open when the low frequency component exceeded a certain threshold. The dead time resulting from each accepted pulse was 400 ns., and low level pulses were rejected.

The outputs of the two pulse standardization systems were fed into a time to amplitude converter (T. A. C.). The T. A. C. produced a signal whose height was proportional to the time difference between the start and stop signals (see figure 9c) only if this difference did not exceed 100 ns. This output pulse was suitably amplified and fed to a 400 channel pulse-height analyzer. Another signal called the valid stop signal which indicated that

a pair of pulses had been analyzed was fed to the slow coincidence system.

The current signal from the dynode was integrated by an operational type preamplifier. The preamplifier signal was in turn amplified to approximately 8 volts by a double delay line amplifier. The gain of the photomultiplier preamp. amplifier system was stabilized by incorporating the photomultiplier high voltage supply into a feedback loop. The high voltage supply incorporated a very stable single channel pulse-height analyzer. A strong line in the pulse-height spectrum was selected and the high voltage supply alternately sampled the counting rate on the high energy and low energy side of the line. An error signal developed from the differences in these counting rates was used to adjust the photo tube high voltage. In this way long time drifts were virtually eliminated from the photomultiplier preamplifier amplifier system.

The signal from each amplifier was fed into two differential discriminators. One of these discriminators selected pulses corresponding to total absorption of the γ ray populating the level under study, and the other selected pulse heights corresponding to total absorption of γ rays depopulating the level. The outputs of these differential discriminators and the valid stop output from the T.A.C. were put into slow triple coincidence as shown in figure 9b. Thus, one slow coincidence unit sensed a coincidence between γ_1, in the fixed detector and γ_2 in the movable detector, and a second coincidence unit served the same function with the roles of the γ rays reversed. A T.A.C. pulse was digitized and stored in the pulse-height analyzer memory when such a slow triple coincidence pulse was present.

The data were recorded by a pulse-height analyzer and a printing scaler. When the system was measuring a change in coincidence counting rate with field direction, the data from the T. A. C. were stored in a certain quadrant of the pulse-height analyzer memory according to table 1. Thus, the rotation of the angular correlation was simultaneously measured at an angle θ in the first half of the memory and at an angle $\pi-\theta$ in the second half of the memory.

When the system was measuring an angular correlation, the T. A. C. signal was routed into the four quadrants of the memory according to the angle between the counters. Thus, the coincidence counting rate measure was the sum of the coincidence counting rate at θ and $\pi-\theta$; however, these two rates were equal since the angular correlation is symmetrical about π.

A typical time spectrum in one of the quadrants of the pulse-height analyzer is shown in figure 10. The peak represents events resulting from γ rays emitted from the same nucleus, and the flat background represents those resulting from different nuclei. Typical time resolutions were 2-3 ns. for the width of the prompt peak.

The experiment was automatically controlled. The configuration of the experiment was changed every 200 seconds by a control system incorporating a quartz oscillator clock. In the case of a rotation measurement the field direction was changed, and in the case of an angular correlation measurement the angle between the detectors was changed.

During each counting period, the number of counts from each of the differential discriminators was recorded in a printing

TABLE 1. Pulse-Height Analyzer Routing Scheme

Coincidence Number 1		Coincidence Number 2	
Field Up	Field Down	Field Up	Field Down
Quadrant 1	Quadrant 2	Quadrant 3	Quadrant 4

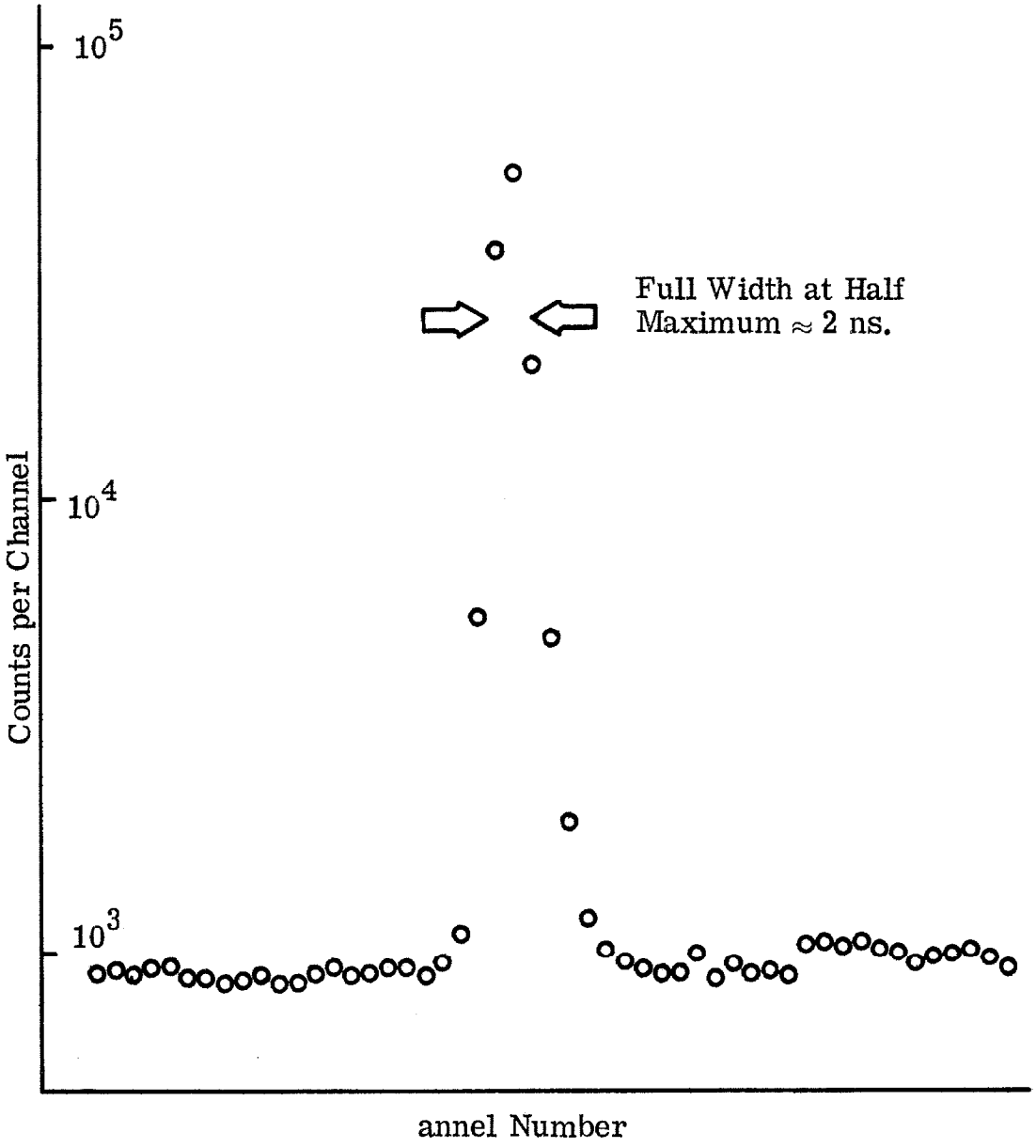

Figure 10. Typical tir o pulse height converter pulse height spectrum as recorde' the pulse height analyzer. Time scale is approximately one annel per nanosecond.

scaler. The fast coincidence counting rate and the field direction were also recorded by the printing scaler. Thus, such quantities as the decay of the source, phase of the experiment and long time drifts were constantly monitored.

4.4 Experimental Procedure

Each measurement consisted of several one day runs. At the end of each run the contents of the pulse-height analyzer memory was read out onto paper tape for future analysis. These data together with the output of the printing scaler were scrutinized for possible indications of malfunction. On the average, the equipment worked satisfactorily 80 percent of the time.

The long term stability of the monitored counting rates was always better than 1 percent. In addition to this good stability, the symmetry of the apparatus led to the cancellation of many potential sources of error. For example, because of the symmetry of the system with respect to γ_1 and γ_2 the finite half life of the radioactive sources used only entered as a second order correlation to the coincidence counting rate as recorded in the pulse-height analyzer. Because of the symmetry, it was possible to measure the angular correlation using the alloy samples, without the necessity of correcting for the perturbation due to the internal fields. Just as the directions of the change in coincidence counting rate in the two halves of the analyzer during a rotation measurement were opposite, the effects of the rotation of the angular correlation due to the randomly oriented fields in the iron cancelled in first order in the sum of coincidences in the angular correlation measurement.

The peak area corrected for random coincidences, and the average number of random counts per channel were determined for each quadrant of the P. H. A. memory. In the case of angular correlation measurements the random counting rate was used to correct the peak area for changes in solid angle due to decentering of the source. In the case of rotation measurements it served as a control experiment.

V. EXPERIMENTAL RESULTS

5.1 Introduction

In this section each of the cases is individually discussed. These cases are the first excited states of ^{114}Cd, the first excited state of ^{122}Te, and the first excited state of ^{124}Te.

5.2 The g Factor of the First Excited State of ^{114}Cd

Indium metal, enriched to 96.4 percent ^{113}In was obtained from Oak Ridge National Laboratory. It was irradiated for seven days in a neutron flux of 2×10^{14} n/cm.^{2}/sec. to produce $^{114}In^m$ activity. Figure 11 gives the energy level diagram of the states in ^{114}Cd populated by the decay of $^{114}In^m$. Also shown are the states populated by Coulomb excitation[19].

The 722, 556 keV cascade was used in this measurement. Figure 12 gives the γ-ray scintillation spectrum of this decay as measured in the previously described apparatus. The lead absorbers were essential in this case in order to reduce the intensity of the 192 keV γ ray to a tolerable level. The range of pulse heights selected by the single-channel analyzers are indicated in figure 12.

There are little data available on the In-Fe system. Although Samoilov[8] used dilute In-Fe alloys in his early investigations of internal fields, he does not fully describe his source preparation techniques. In a preliminary study a .03 atomic percent In-Fe alloy was prepared using inactive indium. The sample was cut into

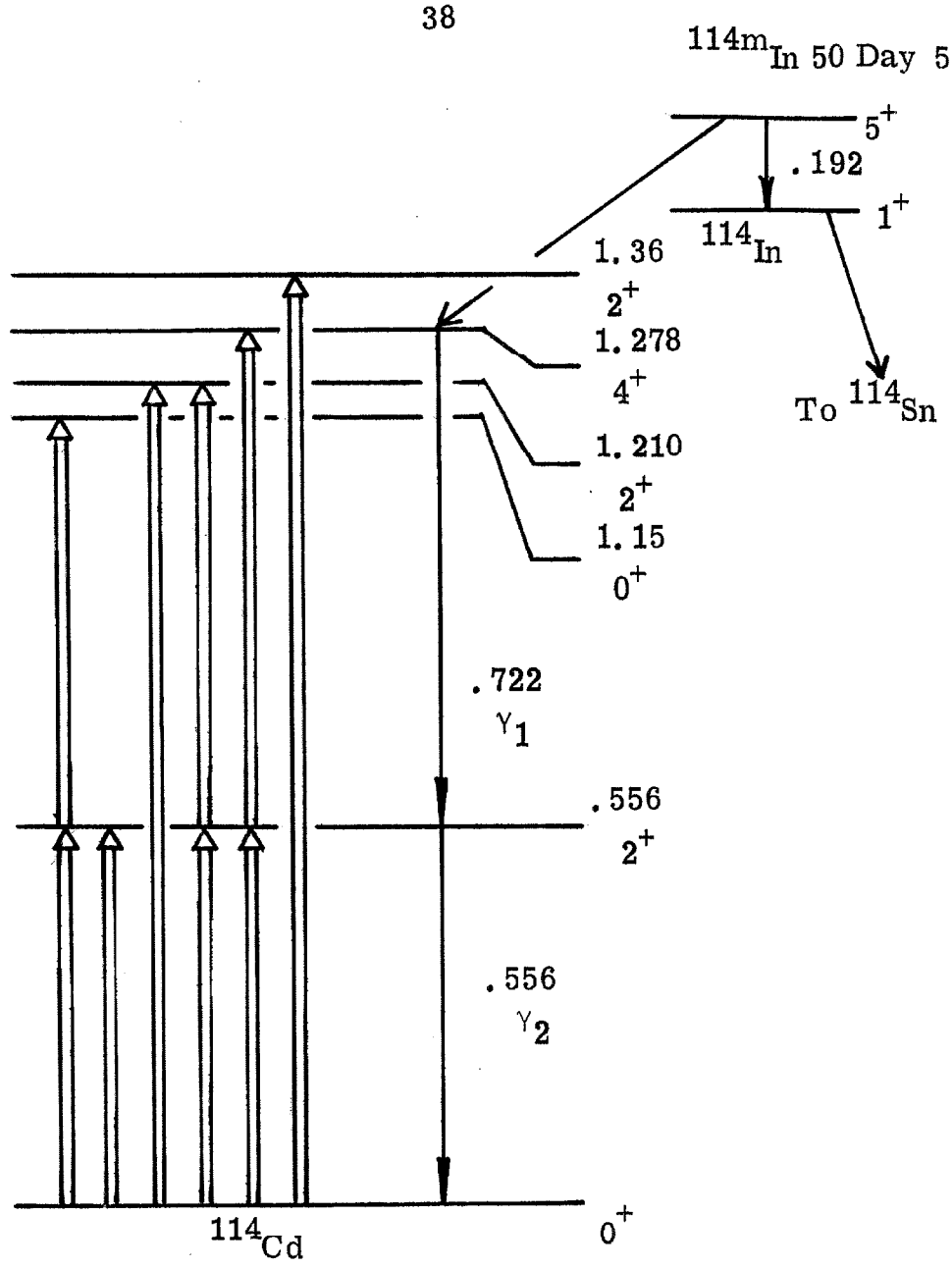

Figure 11. Decay Scheme of $^{114m}In \rightarrow {}^{114}Cd$.

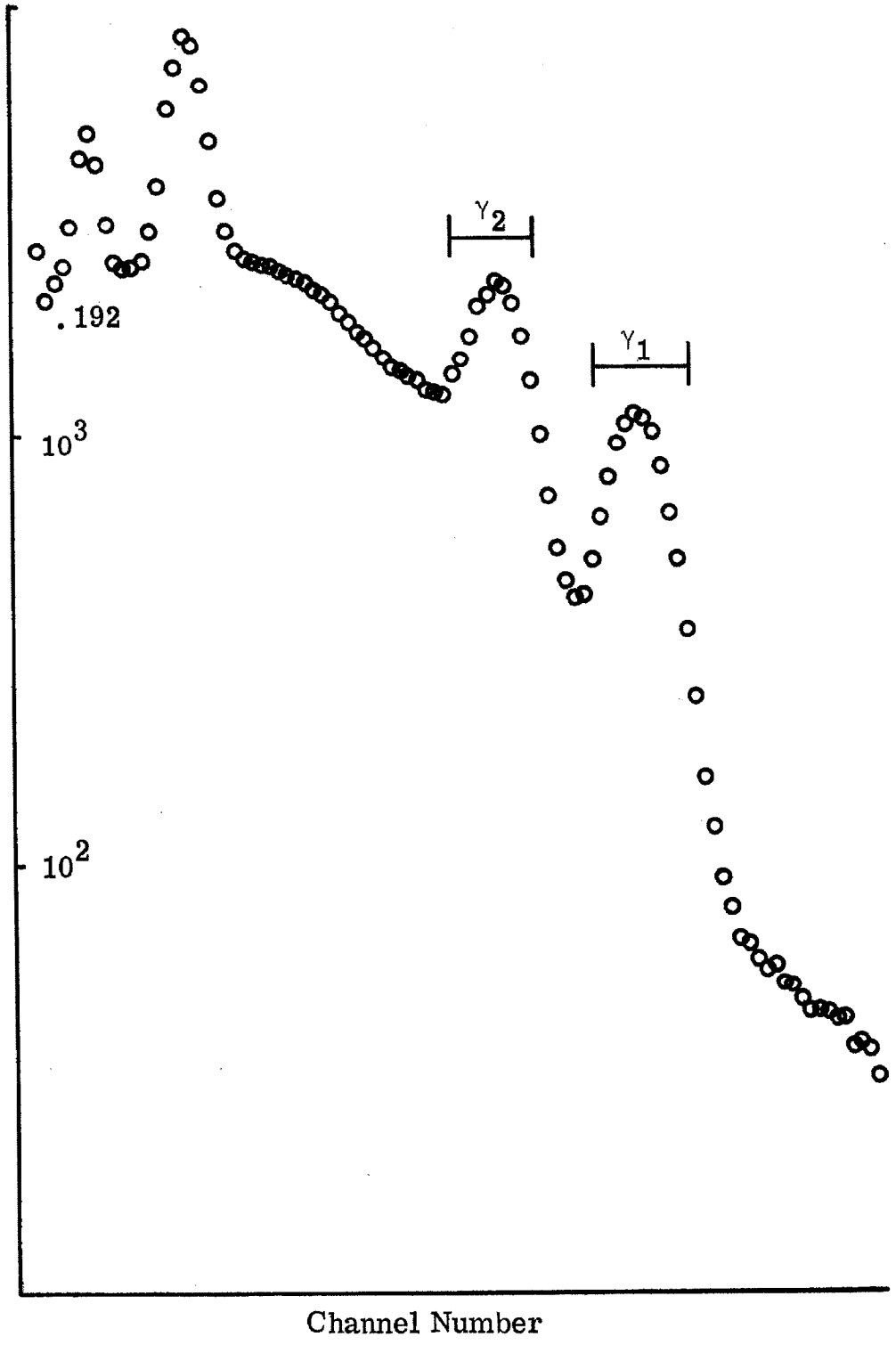

Figure 12. Scintillation Spectrum of $^{114m}In \rightarrow {}^{114}Cd$.

pieces, polished and studied with an electron micro-probe. The indium was found to be homogeneously distributed throughout the sample. The micro-probe spot size was about 1 micron in diameter.

Next, two samples were prepared using active indium. Both samples had indium concentrations of about .007 atomic percent. Sample I was first studied without annealing and then remeasured after annealing for four hours at 1050°C. Source II was annealed for two hours at 850°C. The change in coincidence counting rate at $\theta = 135$ and $\theta = 225$, R(135) and R(225), was measured for each of these sources. As a check on systematic errors R(180) was measured for source I after annealing. The results of these measurements are summarized in table 2 . The three sources evidently gave consistent results; hence, the weighted average of the data appearing in column 1 was used in the determination of the g factor.

The angular correlation between the 722 and 558 keV γ rays was measured several times. The results of these measurements are summarized in figure 13. The angular correlation coefficients ($A_{22} = .084 \pm .001$, $A_{44} = .001 \pm .003$) were not corrected for solid angle. Substituting the final value of R(135) = - R(225) from table 2, $\frac{\partial W(\theta)}{\partial \theta} / W(\theta)$ from figure 13 into formula (8) yields a mean angle of rotation $\omega\tau = +(9.69 \pm 1.06) \times 10^{-2}$ radians.

Several workers have measured the Coulomb excitation cross section from the ground state to the first excited state. These results are summarized by Stelson and Grodzins in ref. (20). They obtain a mean life of $(13.2 \pm .9) \times 10^{-12}$ seconds.

Taking this value for τ and $|H_{int}| = (348 \pm 10)$ kilogauss as measured by Matthias et al. [21] in a perturbed angular experiment

TABLE 2. Summary of ^{114}Cd Data. Values of R are Given in Percent

Source Number	R(135°)	R(225°)	R(180°)	R(Random)
I-unannealed	- . 104 ± . 034	+ . 139 ± . 034		-. 015±. 021
I-annealed	- . 112 ± . 030	+ . 126 ± . 030	+ . 021 ± . 025	+ . 007±. 015
II	- . 155 ± . 033	+ . 130 ± . 033		+ . 019±. 015

Weighted Average $\frac{R(135) - R(225)}{2}$ - . 120 ± . 013

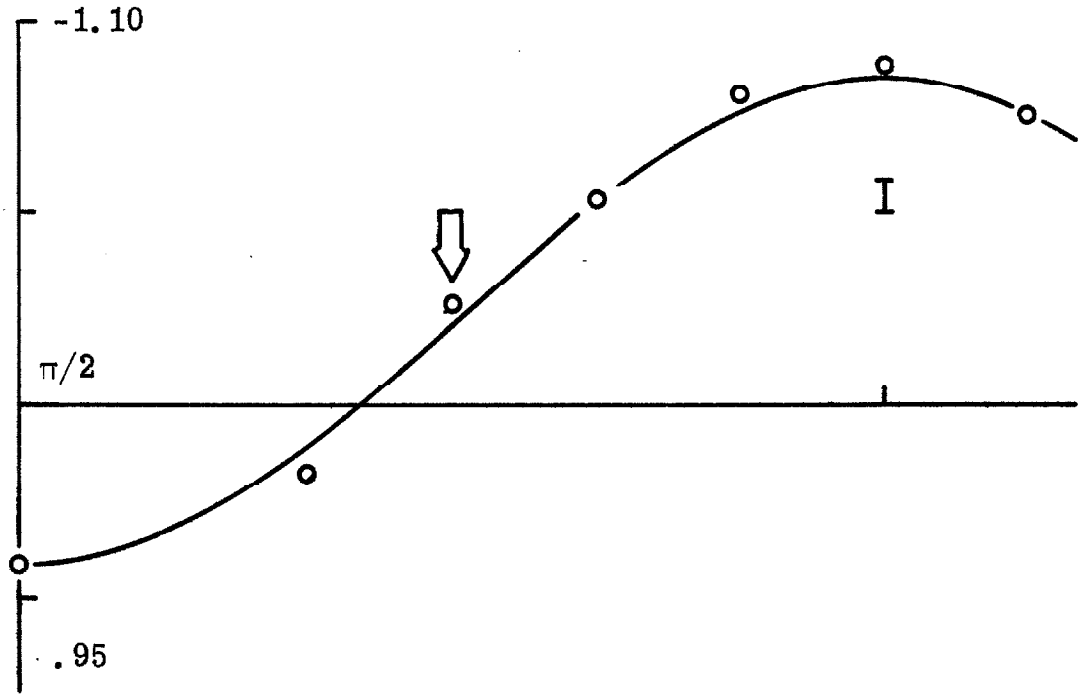

$A_{22} = .0843 \pm .0014$

$A_{44} = .0008 \pm .0030$

$W'/W = .124$

Figure 13. Angular correlation between .722 MeV and .556 MeV γ rays in ^{114}Cd. Data and least-squares fit. The angular correlation coefficients are in agreement with those predicted for a $4^+(E2)2^+(E2)0^+$ cascade with our estimated solid angle correction factors $G_2^1 G_2^2 = .8$ and $G_4^1 G_4^2 = .6$.

using the first excited state of ^{111}Cd, we obtain $|g| = .44 \pm .06$ nuclear magnetons, corresponding to $|\mu_2| = .88 \pm .12$ nuclear magnetons, since the spin of the state is 2. It seems reasonable to assume that H_{int} varies smoothly with Z, hence from figure 3 one would predict a negative sign for the field of Cd in Fe. This assumption leads to a positive g factor and magnetic moment.

5.3 First Excited State of ^{122}Te

Several samples of antimony metal enriched to 98.4 percent ^{121}Sb were irradiated for two days in a flux of 2×10^{14} n/cm.^{2}/sec. to produce the 2.8 decay ^{122}Sb activity used in this experiment. Figure 14 gives the energy level diagram of states in ^{122}Te populated by the decay of ^{122}Sb (22). The 686, 564 keV cascade was used in this experiment. Figure 15 gives the scintillation spectrum resulting from this decay and indicates the window settings used. The 1.69 MeV photo peak resulting from the decay of ^{124}Sb to ^{124}Te is also apparent in this decay. This spectrum represents the largest contamination encountered in any of the runs. The estimated coincidence counting rate due to the ^{124}Sb activity is 2 percent of the ^{122}Sb rate.

The rotation of this state in the internal field of iron has been observed in three earlier experiments. Johansson et al. (23) find $\omega\tau = -(0.0132 \pm .0013)$ radians in a γ-γ correlation measurement. Their source was prepared by electropolating ^{122}Sb activity on an iron cylinder, diffusing the activity into the iron at 900°C for twelve hours, and then dissolving away the surface activity with

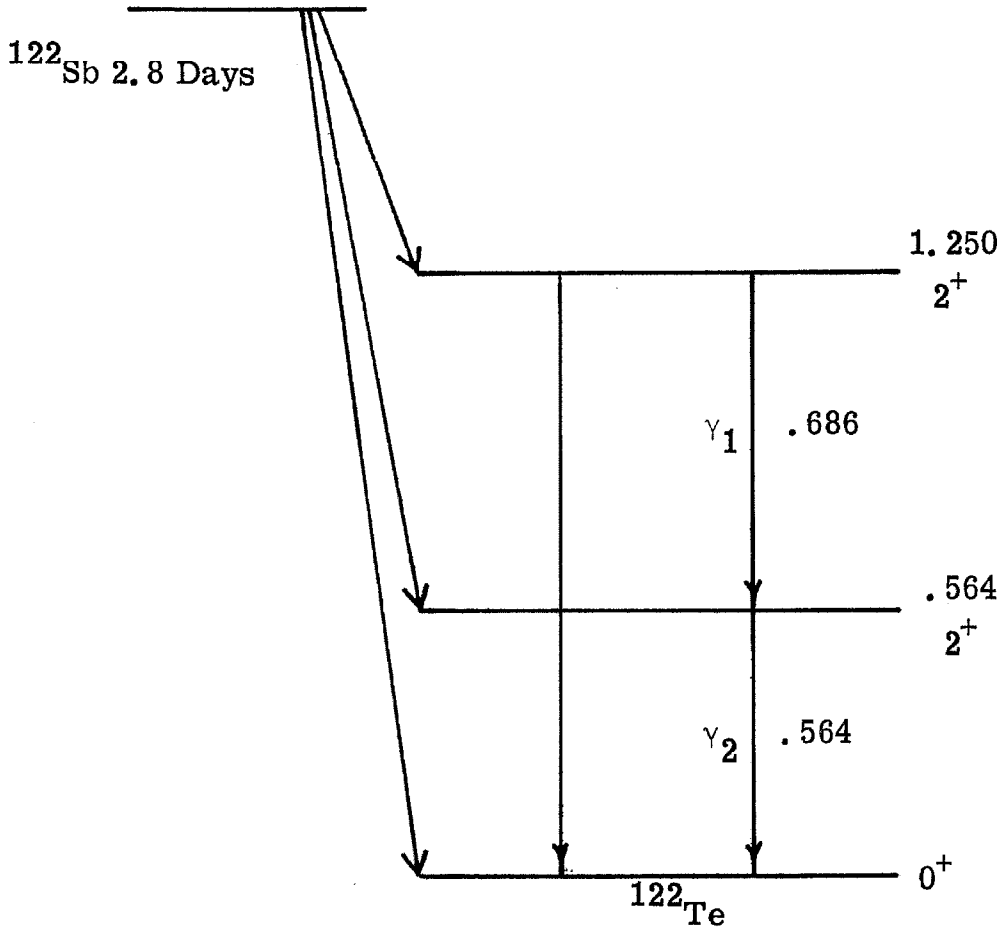

Figure 14. Decay Scheme of ^{122}Sb → ^{122}Te.

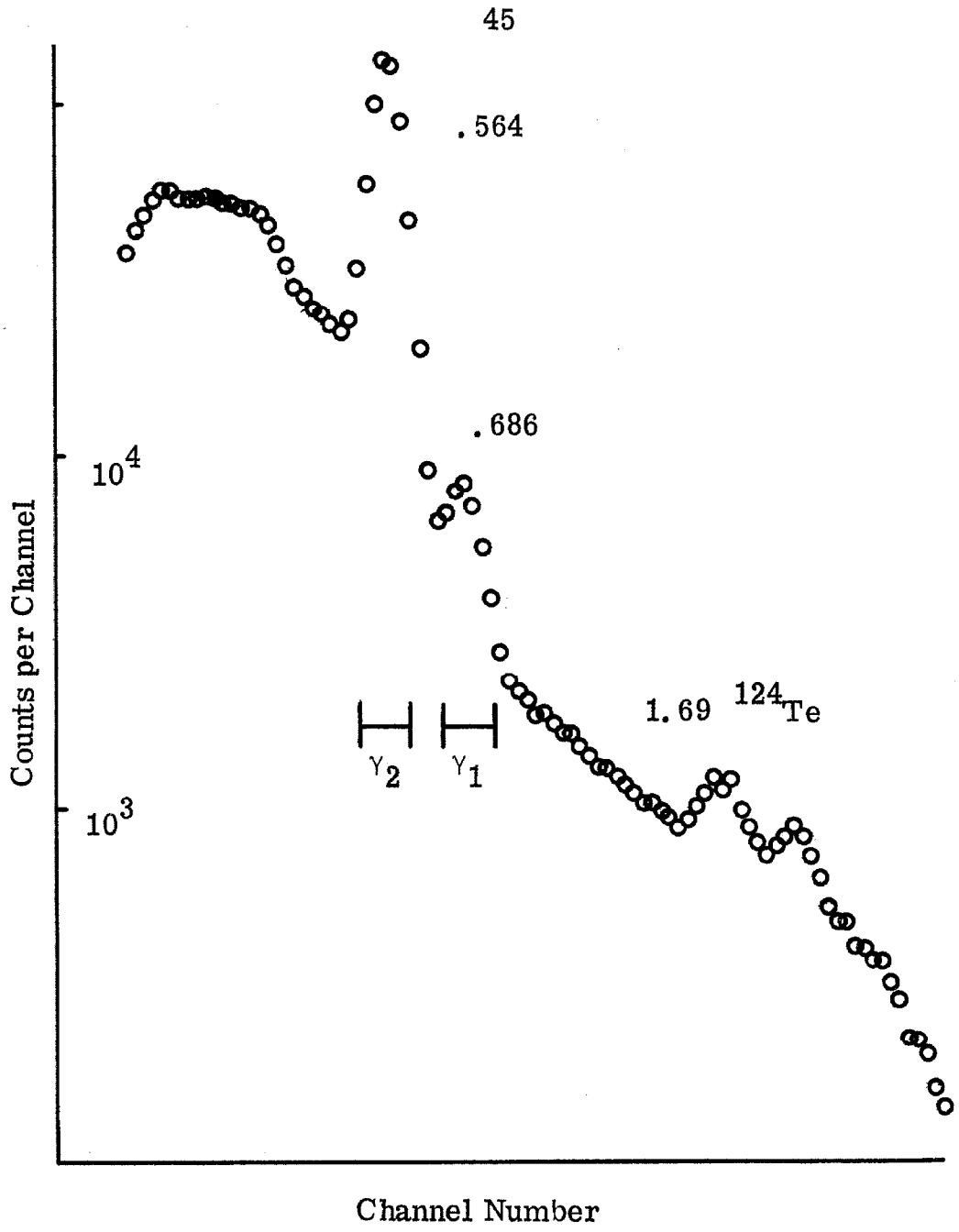

Figure 15. Scintillation spectrum of $^{122}Sb \rightarrow {}^{122}Te$.

aqua regia. Auerbach et al.[24] in a similar experiment find $\omega\tau$ = - (0.0154 ± .015) radians. Their source had a concentration of less than one atomic percent, and was prepared by melting ^{122}Sb with iron in an argon atmosphere. The annealing procedure is not specified. Borchers et al.[4] find $\omega\tau$ = - (0.0177 ± .0012) radians using a Coulomb excitation technique.

The agreement between these three values is poor. Our purpose in the measurement of the ^{122}Te g factor was, therefore, twofold; to improve the statistical error on the value of the g factor, and to investigate the effect of source preparation procedure on the measured value of $\omega\tau$.

Three source samples were prepared. Source I was .007 atomic percent antimony in iron, and was annealed for two hours in vacuum at 850°C. Source II was of similar composition but was annealed at 1050°C. Source III was approximately one atomic percent antimony and was annealed at 850°C. Figure 16 gives the Sb-Fe phase diagram for small antimony concentrations as given in Hansen[25]. The room temperature solubility of antimony in iron has not been accurately established. Hagg[26] reports a solubility of three atomic percent. Geller[27] reports 2.4 atomic percent. In the fabrication of our own alloys, we observed that the dilute alloys had perceptibly the same mechanical properties as iron, but that the one atomic percent alloy was brittle and shattered upon impact. A possible interpretation of this observation is that some antimony had precipitated at grain boundaries. In any case the antimony concentration of our alloys was well below either solubility quoted above.

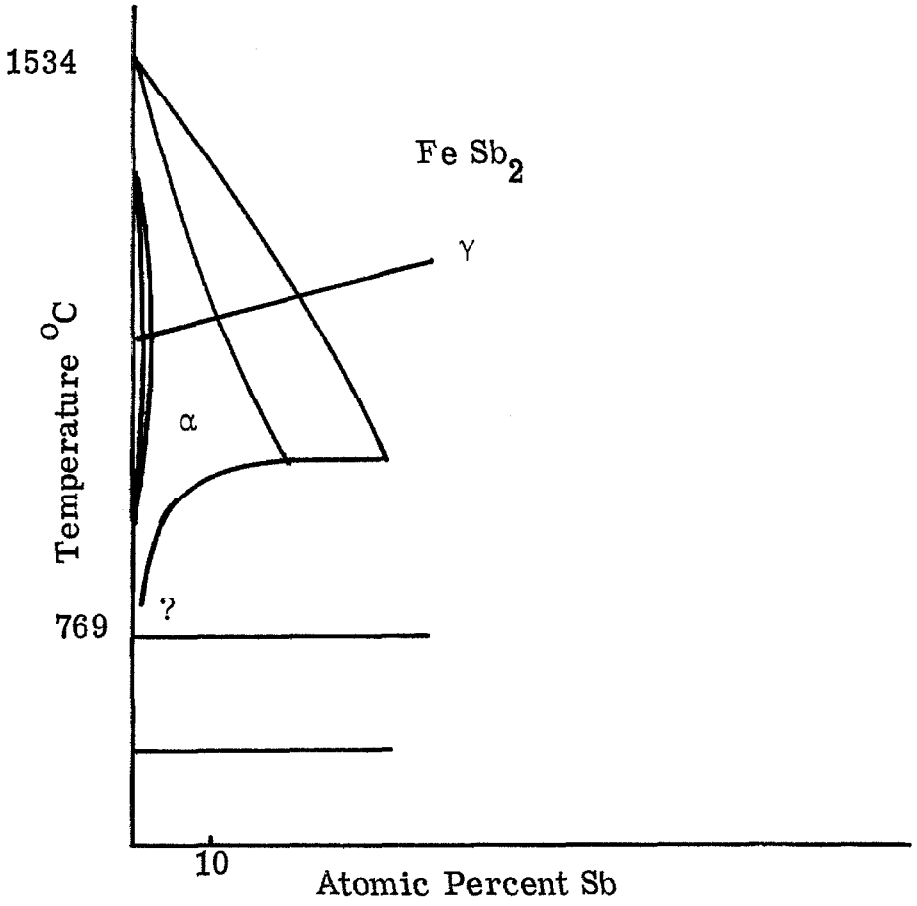

Figure 16. Phase diagram of the Sb-Fe system for small concentrations of Sb.

The experimental results are summarized in figure 17 which gives the angular correlation results, and table 3 which gives the values of R(157.5) and R(202.5) for each of the samples and the results of control experiments. The values of $\omega\tau$ obtained for the dilute alloys are consistent and are in agreement with the results of Johansson et al. Our results are in poor agreement with the value for $\omega\tau$ obtained by Auerbach et al., who obtain a value larger than ours. The one atomic percent alloy gives a somewhat smaller effect than the dilute alloys, and hence a concentration dependence of the field cannot explain the poor agreement between our results and those of Auerbach et al. who obtain a larger effect. Our result is in definite disagreement with that of Borchers et al.[4] obtained by the Coulomb excitation technique. The weighted average of our dilute alloy results gives $\omega\tau = -(1.02 \pm .07) \times 10^{-2}$ radians.

The lifetime of this state has been measured by several workers. As before, we adopt the weighted average as determined by Stelson and Grodzins, who give $\tau = (11.0 \pm 1.1) \times 10^{-12}$ seconds. The magnetic field of Te in Fe has been measured by Frankel et al.[9] to be $+(620 \pm 20)$ kilogauss at $4^{\circ}K$. If we assume the field is proportional to the bulk magnetization, then we obtain an internal field of $+(605 \pm 20)$ kilogauss. Using these values of τ and H_{int} we obtain $g = .31 \pm .03$ nuclear magnetons, and $\mu = .62 \pm .03$ nuclear magnetons.

5.4 The g Factor of the First Excited State of ^{124}Te

Antimony metal enriched to 97.7 atomic percent ^{124}Sb was irradiated for twenty days in a neutron flux of 5×10^{14} n./cm.^{2}/sec.

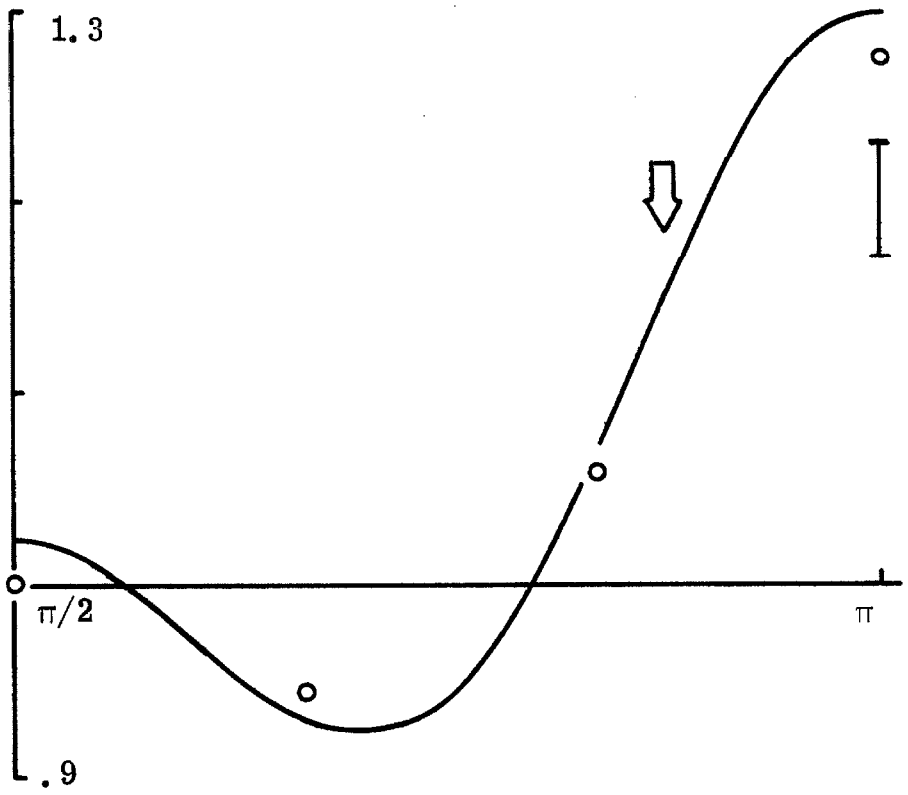

$A_{22} = .1012 \pm .0018$

$A_{44} = .1987 \pm .0035$

$W'/W = .532 \pm .010$

Figure 17. Angular correlation between .686 MeV and .564 MeV γ rays in ^{122}Te. Data and least-squares fit.

TABLE 3. Summary of ^{122}Te Data. Values of R are Given in Percent

Source Number	R(157.5°)	R(202.5°)	R(Random)
I	.616 ± .082	- .536 ± .082	.000 ± .025
II	.445 ± .089	- .619 ± .090	.030 ± .040
III	.425 ± .110	- .324 ± .112	-.027 ± .080

Source Number	$\frac{R(157.5^{\circ})-R(202.5^{\circ})}{2}$	$\omega\tau$(Radians)
I	.576 ± .058	$(1.05 \pm .10) \times 10^{-2}$
II	.532 ± .063	$(.99 \pm .11) \times 10^{-2}$
III	.375 ± .078	$(.70 \pm .14) \times 10^{-2}$

Weighted average of data from I and II

.555 ± .036	$(1.02 \pm .07) \times 10^{-2}$

to form the 60 day ^{124}Sb activity used in the experiment. Figure 18 gives the energy levels in ^{124}Te populated by this decay[28]. Figure 19 gives the scintillation spectrum of ^{124}Te as observed in our detectors. The source used in these measurements was similar to source I in the ^{122}Te experiment.

Two experiments were performed; the first using the 1.69 - .603 MeV cascade, the second using the .772 - .603 MeV cascade. The window settings used in these measurements are indicated on figure 19. Obviously Compton events from higher energy rays will be accepted in the 1.69 MeV and .722 MeV windows. This fact makes the interpretation of the angular correlation results difficult, but does not affect the rotation measurement, since all strong γ rays terminate in the .603 MeV level.

The results of the angular correlation experiments for the two window settings previously indicated are summarized in figures 20 and 21. R(135) and R(225) were measured for the 1.69 - .603 MeV cascade. R(157.5) and R(202.5) were measured for the .722 - .603 MeV cascade. The results of these experiments and associated control experiments are presented in tables 4 and 5. In the former experiment we obtain $\omega\tau = -(.66 \pm .24) \times 10^{-2}$ radians and in the latter $\omega\tau = -(.54 \pm .13) \times 10^{-2}$ radians.

This state has also been studied by Borchers et al.[4] using the Coulomb excitation technique. They find $\omega\tau = -(1.48 \pm .09) \times 10^{-2}$ radians. The two results disagree. Possible reasons for this disagreement will be discussed in a later section.

Using our value for $\omega\tau$, a lifetime of $(6.0 \pm 1.2) \times 10^{-12}$ seconds from Stelson and Grodzins, and a field of 605 ± 20 kilogauss as in the case of ^{122}Te we obtain g = .22 ± .05 nuclear magnetons.

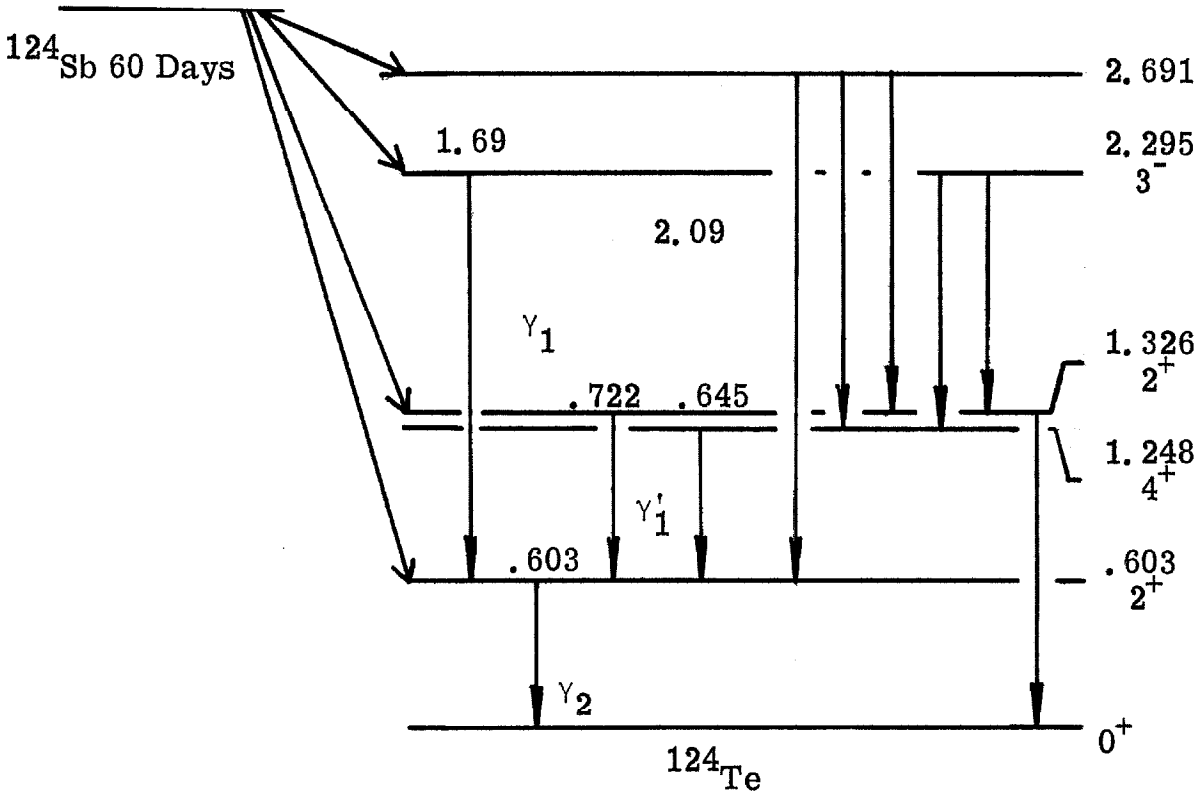

Figure 18. Decay scheme of $^{124}Sb \rightarrow {}^{124}Te$, showing only intense γ rays.

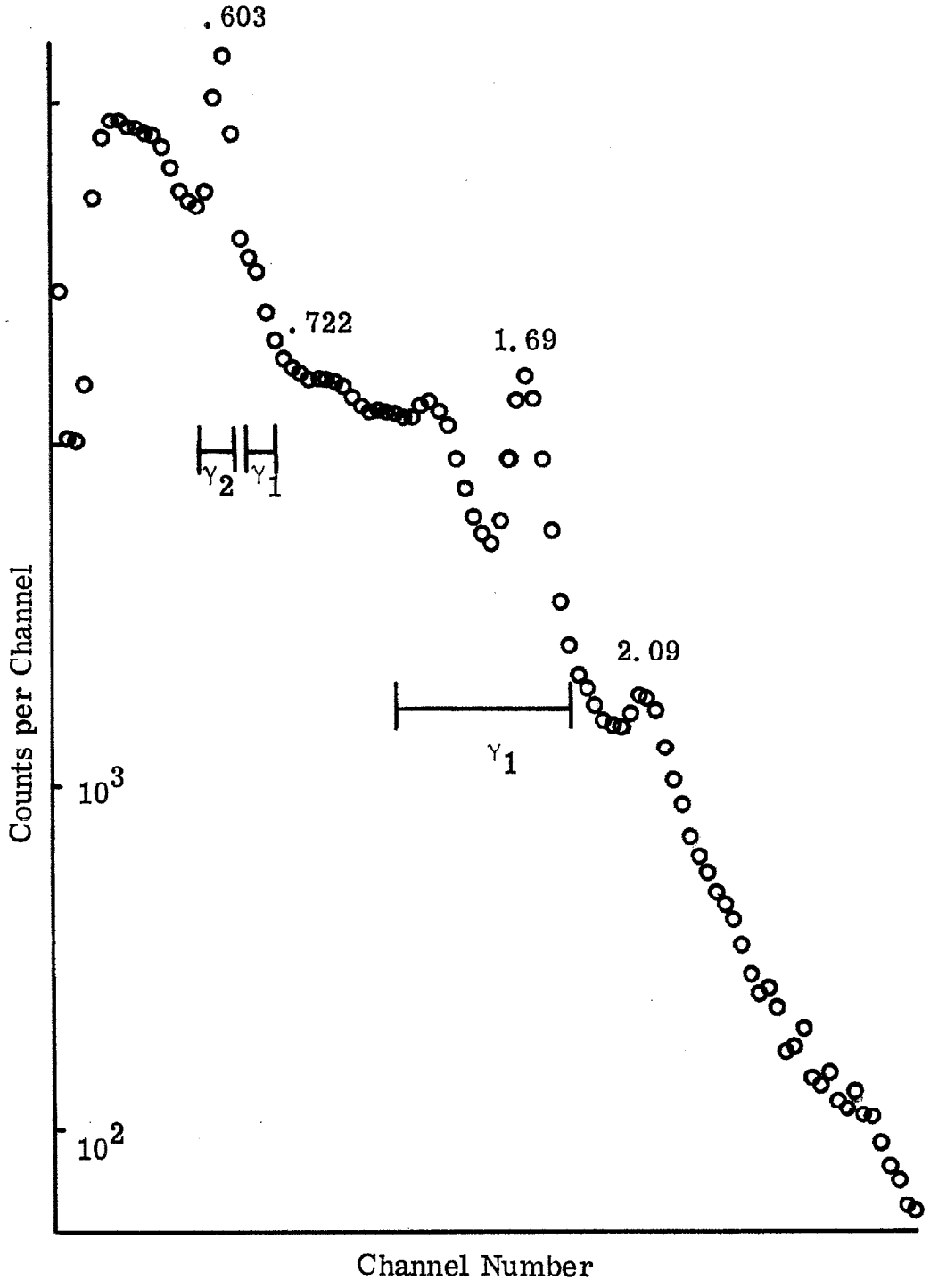

Figure 19. Scintillation spectrum of $^{124}Sb \rightarrow {}^{124}Te$.

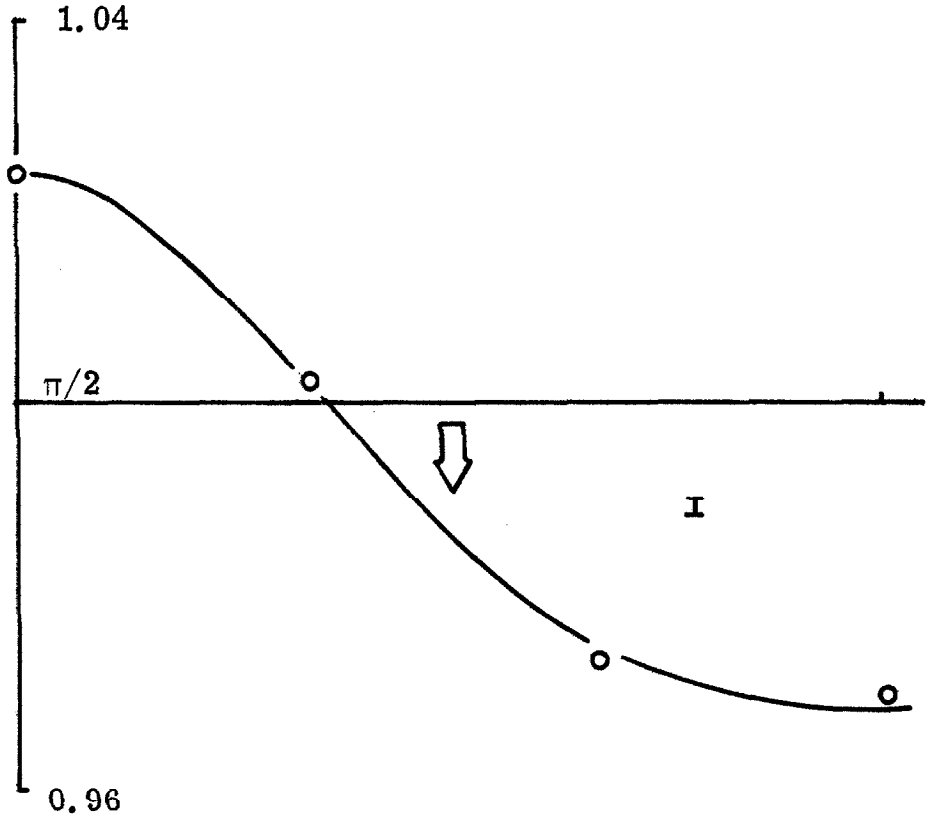

$A_{22} = -.0411 \pm .0008$
$A_{44} = +.0093 \pm .0008$
$W'/W = -.0566 \pm .0010$

Figure 20. Angular correlation between 1.69 MeV and .603 MeV γ rays in ^{124}Te. Data and least-squares fit.

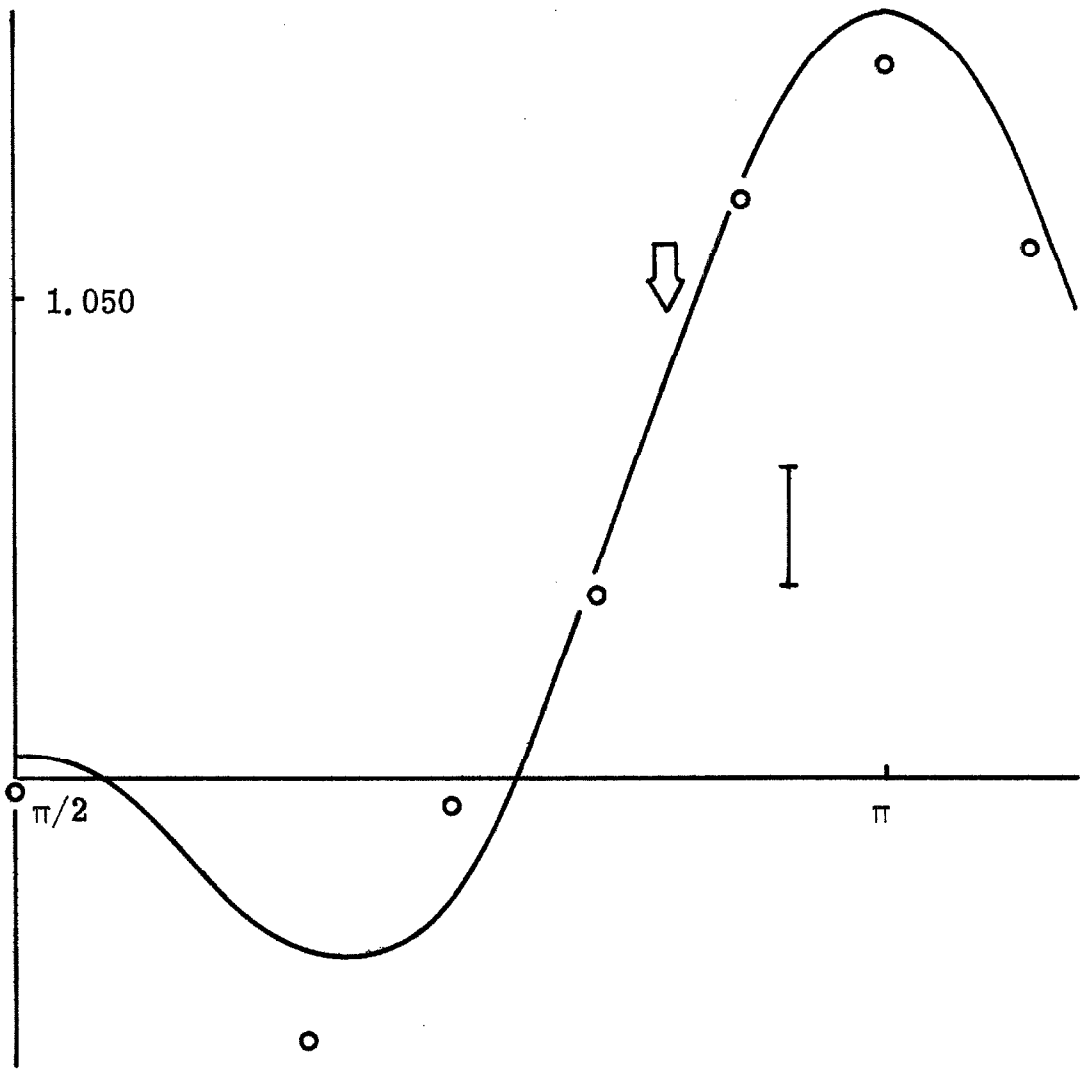

$A_{22} = .0315 \pm .0011$
$A_{44} = .0486 \pm .0014$
$W'/W = .154 \pm .004$

Figure 21. Angular correlation between .722 MeV and .603 MeV γ rays in ^{124}Te. Data and least-squares fit.

TABLE 4. Summary of ^{124}Te Data From 1.69, .603 MeV Cascade. Values of R are Given in Percent

R(135°)	R(225°)	R(180°)	R(Random)
- .040 ± .014	+ .031 ± .014	- .021 ± .019	.007 ± .011

$$\frac{R(135^{\circ})-R(225^{\circ})}{2} = .037 \pm .010$$

$$\omega\tau = (.66 \pm .24) \times 10^{-2} \text{ radians}$$

TABLE 5. Summary of ^{124}Te Data From .722, .603 MeV Cascade. Values of R are Given in Percent

R(157.5°)	R(202.5°)	R(180°)	R(Random)
.088 ± .030	- .080 ± .030	- .024 ± .028	.008 ± .023

$$\frac{R(157.5^{\circ})-R(207.5^{\circ})}{2} = .084 \pm .021$$

$$\omega\tau = -(.54 \pm .13) \times 10^{-2} \text{ radians}$$

VI. COMPARISON WITH THE RESULTS OF COULOMB EXCITATION IMPLANTATION EXPERIMENTS

Values have been obtained by Borchers et al.[4] for the first 2^+ states in ^{120}Te, ^{122}Te, ^{124}Te, ^{126}Te and ^{128}Te. They used the Coulomb excitation method which has been referred to above. In these experiments the Te nuclei are Coulomb excited by heavy ions and forward scattered into an iron field. The precession of the angular correlation between back scattered ions and the γ ray de-exciting the first excited state is observed.

These $\omega\tau$ values are plotted as a function of excited state lifetime in figure 22. Our results for ^{122}Te and ^{124}Te are also included. Herskind et al.[29] have performed similar experiments on the first 2^+ levels in ^{104}Pd, ^{106}Pd, ^{108}Pd and ^{110}Pd. These results, together with the angular correlation results of Auerbach et al.[30] which has been verified in this laboratory[31] are plotted against the lifetime of the excited state in figure 23. In each figure, there is evident disagreement between the results of the Coulomb excitation and the angular correlation experiments.

Static magnetic fields appropriate to the atomic ground state have been assumed in the analysis of the Coulomb excitation data. While the Coulomb excited nuclei are stopping the atom is certainly not in its ground state. Borchers et al. have estimated a stopping time of 7×10^{-13} seconds for the Te nuclei in their experiments. Further, some time is required for the atoms to find lattice positions, de-ionize, and decay to their ground state once they have stopped. While these processes are taking place, the internal field will not be the static field as measured by other methods.

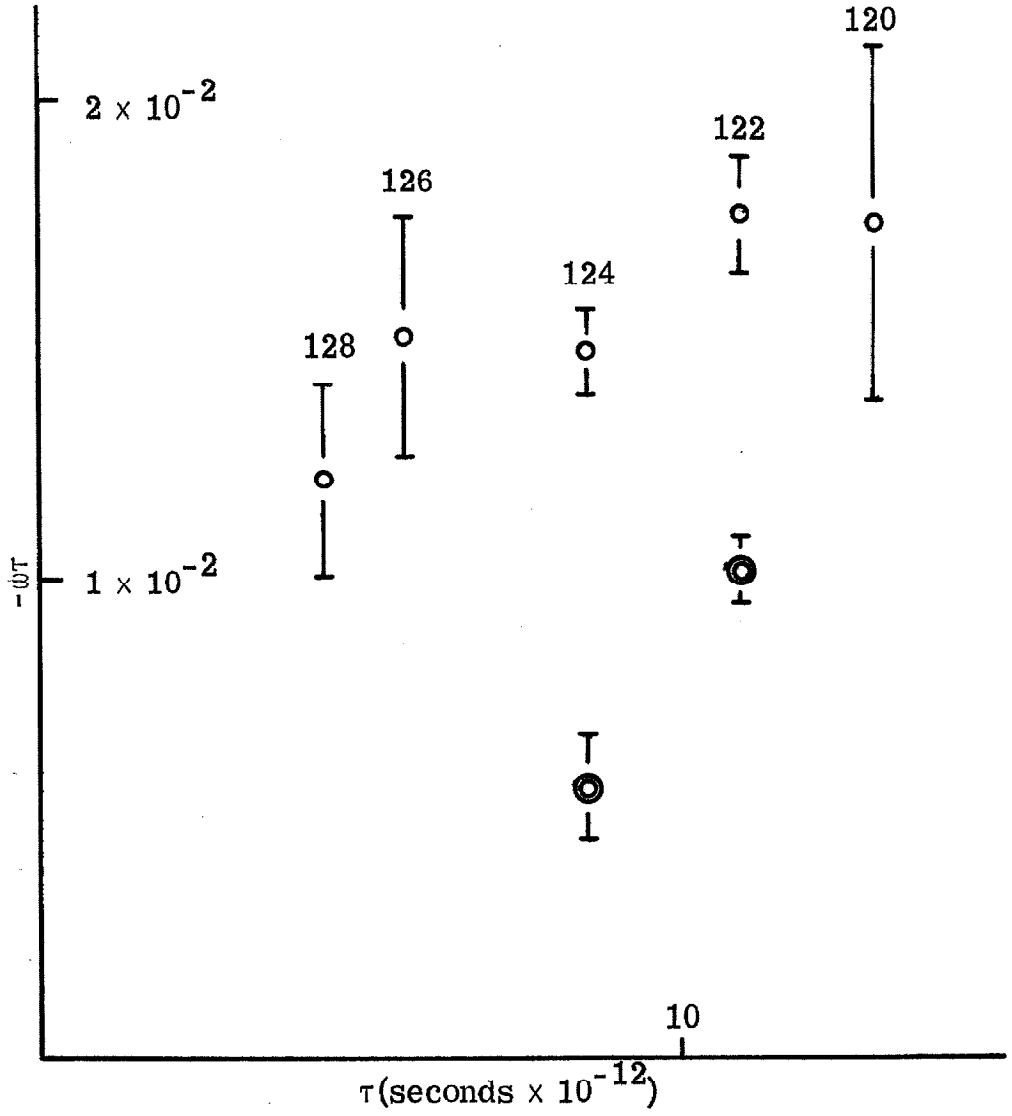

Figure 22. Plot of $\omega\tau$ vs. τ for first 2^+ states in Te isotopes. Single circles are Coulomb excitation implantation values and double circles are the angular correlation results reported in this thesis.

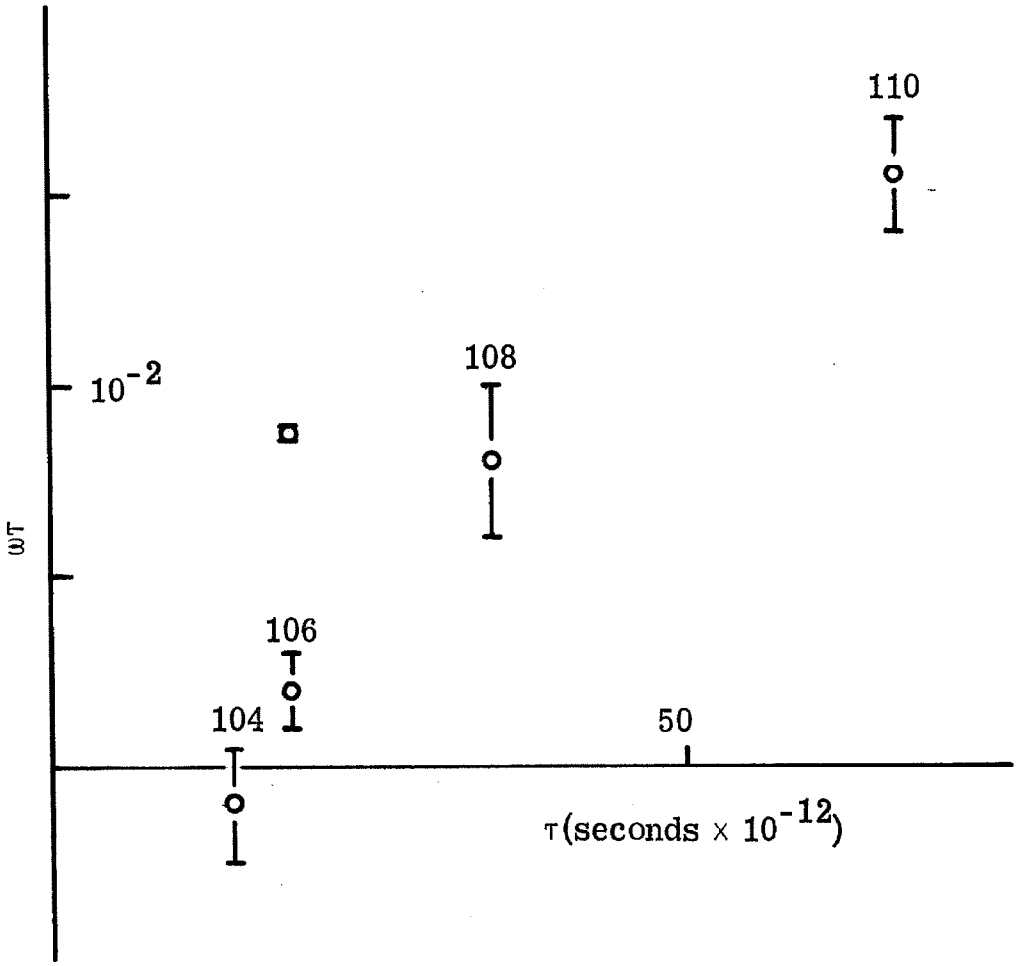

Figure 23. Plot of ωτ vs. τ for first 2^+ states in Pd isotopes. The point with small error bars is the angular correlation result of Auerbach. The other points are values obtained by Coulomb excitation implantation measurements.

If we make the approximations that the stopping time is small compared to the excited state lifetime, and that the g factors of the states are the same, then the relationship between the $\omega\tau$ values measured by Coulomb excitation and those measured by γ-γ angular correlation methods becomes $\omega\tau_{CE} = \omega\tau_{AC} + \theta_0$ where θ_0 is the angle of rotation which the Coulomb excited nuclei undergo while stopping. This model predicts that the intercept on the $\omega\tau$ axis of the Coulomb excitation results of figures 22 and 23 should be equal to the differences between the $\omega\tau$ values measured by the two techniques for each isotope. This conclusion is borne out by the data presented in figures 22 and 23.

The explanation given above for the discrepancies between the results of the two techniques could be tested by measuring $\omega\tau$ as a function of the recoil energy of the Coulomb excited particle.

VII. COMPARISON WITH THEORY

In 1955 Sharff - Goldhaber and Weneser[32] suggested that the properties of the low-lying energy levels in medium weight ($36<N<108$) even-even nuclei could be understood in terms of the vibrational model first proposed by Bohr and Mottelson[33]. This model assumes that the low-lying excited states can be described as quadrupole vibrations about a spherical equilibrium shape.

Most of the spectroscopic characteristics of the nuclei ^{114}Cd, ^{122}Te, and ^{124}Te are in qualitative agreement with the vibrational model. Thus, the ground state is 0^+, the first excited state is 2^+, and a 0^+, 2^+, 4^+ triad is found at about two times the energy of the first 2^+ state. Gamma-ray transitions between states differing by one phonon are strong, and transition between states differing by two phonons, which are forbidden in the vibrational model, are relatively weak. The B(E2)'s of the one and two phonon transitions are given in table 6[34].

There are important deviations from the characteristics predicted by the vibrational model. In the nuclei we have studied, and in general, the 0^+, 2^+, 4^+ triad is not degenerate, and its center of energy is more than twice the energy of the first excited 2^+ state. The observed ratios of allowed B(E2)'s do not agree with those predicted by the model ($B(B_2, I \rightarrow 2^+)/B(E_2, 2^+ \rightarrow 0^+) = 2$, and the two phonon transition $2^{+'} \rightarrow 0^+$ ($2^{+'}$ denotes the second excited 2^+ state) is weak but nonetheless present. However, the most striking deviation from the vibrational model is the large experimentally observed static electric quadrupole moment of the first excited state in ^{114}Cd. This measurement was first performed at Caltech by

TABLE 6. Summary of Quadrupole Transition Rate Data

Nuc.	$B(E2,2^+\rightarrow 0^+)$ S. P. U.	$\frac{B(E2,2^{+\prime}\rightarrow 2^+)}{B(E2,2^+\rightarrow 0^+)}$	$\frac{B(E2,4^+\rightarrow 2^+)}{B(E2,2^+\rightarrow 0^+)}$	$\frac{B(E2,0^{+\prime}\rightarrow 2^+)}{B(E2,2^+\rightarrow 0^+)}$	$\frac{B(E2,2^{+\prime}\rightarrow 0^+)}{B(E2(2^+\rightarrow 0^+)}$
^{114}Cd	34.6 ± 2.5	1.2 ± .2	1.80 ± .23	.85 ± .17	.015 ± .005
^{122}Te	36.4 ± 3.5	3.1 ± .5			.009 ± .003
^{124}Te	33.2 ± 6.6				.009 ± .002
Vib. Model	Large	2	2	2	0

de Boer et al.[35], and later repeated by Stelson et al.[36] and Simpson et al.[37]. A weighted average of their results yields $Q_2 = (-.5 \pm .25)$ barns. This value of Q_2 might be expected in the region of deformed nuclei, but since the quadrupole operator is a linear combination of phonon creation and annihilation operators, its expectation value for states of a definite number of phonons must vanish.

Tamura and Udagawa[2] have recently attempted to explain this large quadrupole moment, while retaining the vibrational character of the ^{114}Cd nucleus. They propose two models which predict quite different magnetic moments for the first 2^+ state.

Model one, a phenomenological model, considers the first and second 2^+ states to be a combination of one and two phonon states. The mixing ratio of one and two phonon states and the amplitude of the vibrations are adjusted to fit R_1, the ratio of the energies of the second and first 2^+ states and $B(E2, 2^+ \rightarrow 0^+)$. The magnitude of the quadrupole moment and $R_2 = B(E2, 2^+ \rightarrow 0^+)/B(E2, 2^+ \rightarrow 0^+)$ are then calculated. It is assumed that the interaction causing the mixing does not alter the hydrodynamic model value for the g factor, Z/A.

Model two, a microscopic model, calculates the above properties (g, R_1, R_2, Q_L) on the basis of a pairing force together with a long range quadrupole force. In a preliminary calculation, Tamura and Udagawa show that in order to obtain a sufficiently large quadrupole moment it is necessary to have a larger mixing of one and two phonon states than the usually employed mathematical approximations will allow. They, therefore, have included

previously neglected higher order terms in their microscopic calculation. In table 7 the predictions of the two models for (g, R_1, R_2, and Q_2) are summarized and the results of experiments are given. Evidently neither model is successful in predicting all of the experimental quantities, although they both predict sufficiently large quadrupole moments for the first excited state. The phenomenological model leads to a two phonon transition too fast by a factor of 9, and the microscopic model predicts a g factor too large by a factor of 2.

The calculation of g factors of the first excited states in ^{122}Te and ^{124}Te have been carried out by Kisslinger and Sorensen[3]. They were not concerned with the quadrupole moments, which are not measured, but do give predictions for B(E2, $2^+ \rightarrow 0^+$) and B(E2, $2^{+'} \rightarrow 0^+$). They consider a short range pairing force together with a long range quadrupole force. The pairing force constant is taken as equal for neutrons and protons and is extrapolated from Sn isotopes assuming a 1/A dependence. The quadrupole force constant is adjusted to give the correct energy for the first excited 2^+ state. A comparison between the predictions of Kisslinger and Sorensen for the nuclear quantities mentioned above (g, B(E2, $2^+ \rightarrow 0^+$), B(E2, $2^{+'} \rightarrow 0^+$) and the results of experiment is given in table 8. The one phonon and two phonon transition rates are in qualitative agreement with the experiment, and the deviations of the g factor from Z/A are in the right direction, but are too large. As Kisslinger and Sorensen suggest, this discrepancy may be due to the fact that they completely neglect contributions from the closed shells, which would tend to bring the g factor closer to Z/A.

TABLE 7. Comparison of the Predictions of Tamura and Udagawa for the Properties of the Low-Lying Levels of ^{114}Cd With Experiment

Quantity	Phenomological Model	Microscopic Model	Experiment
$g(\mu_N)$	.43	1.19	.44 ± .06
R_1	1.2	1.65	1.25 ± .25
R_2	.14	.047	.015 ± .005
Q(barns)	$\|Q\| = .58$	-.439	-.5 ± .25

TABLE 8. Comparison of the Predictions of Kisslinger and Sorensen with Experiment

^{122}Te

Quantity	Prediction	Experiment
$g(\mu_N)$	.17	.31 ± .03
$B(E2, 2^+ \rightarrow 0^+)$(s. p. u.)	35.	36.4 ± 2.5
$B(E2, 2^{+'} \rightarrow 0^+)$(s. p. u.)	.24	.10 ± .02

^{124}Te

$g(\mu_N)$	.16	.22 ± .05
$B(E2, 2^+ \rightarrow 0^+)$(s. p. u.)	21.	33.2 ± 6.6
$B(E2, 2^{+'} \rightarrow 0^+)$(s. p. u.)	.16	.10 ± .02

The predictions of Kisslinger and Sorensen, those of Tamura and Udagawa, and the semi-classical estimate Z/A, are compared with our experimental results in figures 24a, b. Kisslinger and Sorensen's predictions for other first 2^+ vibrational states in this region are also given.

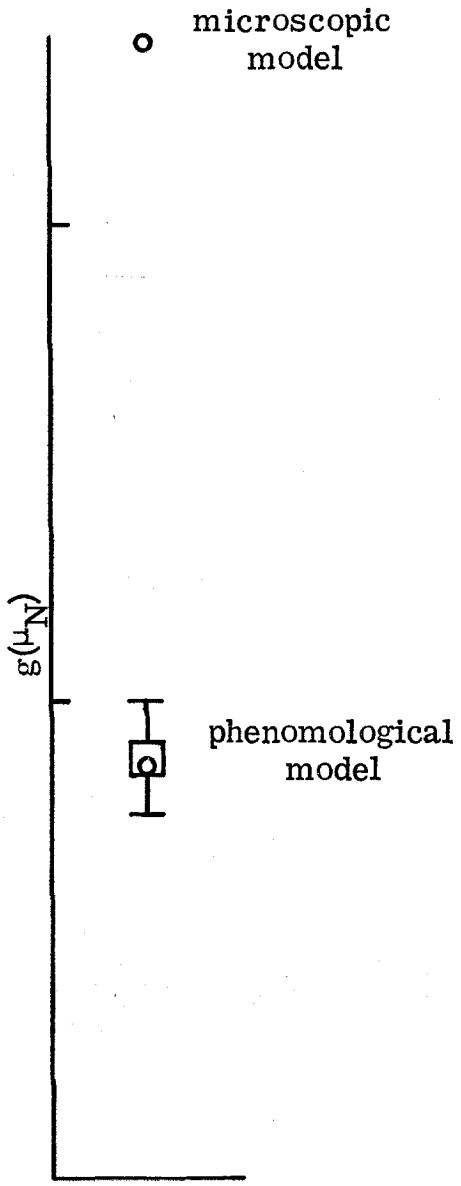

Figure 24a. Predictions of the phenomological and microscopic models of Tamura and Udagawa for the g factor of the first 2^+ state in ^{114}Cd. Our experimental value is also given.

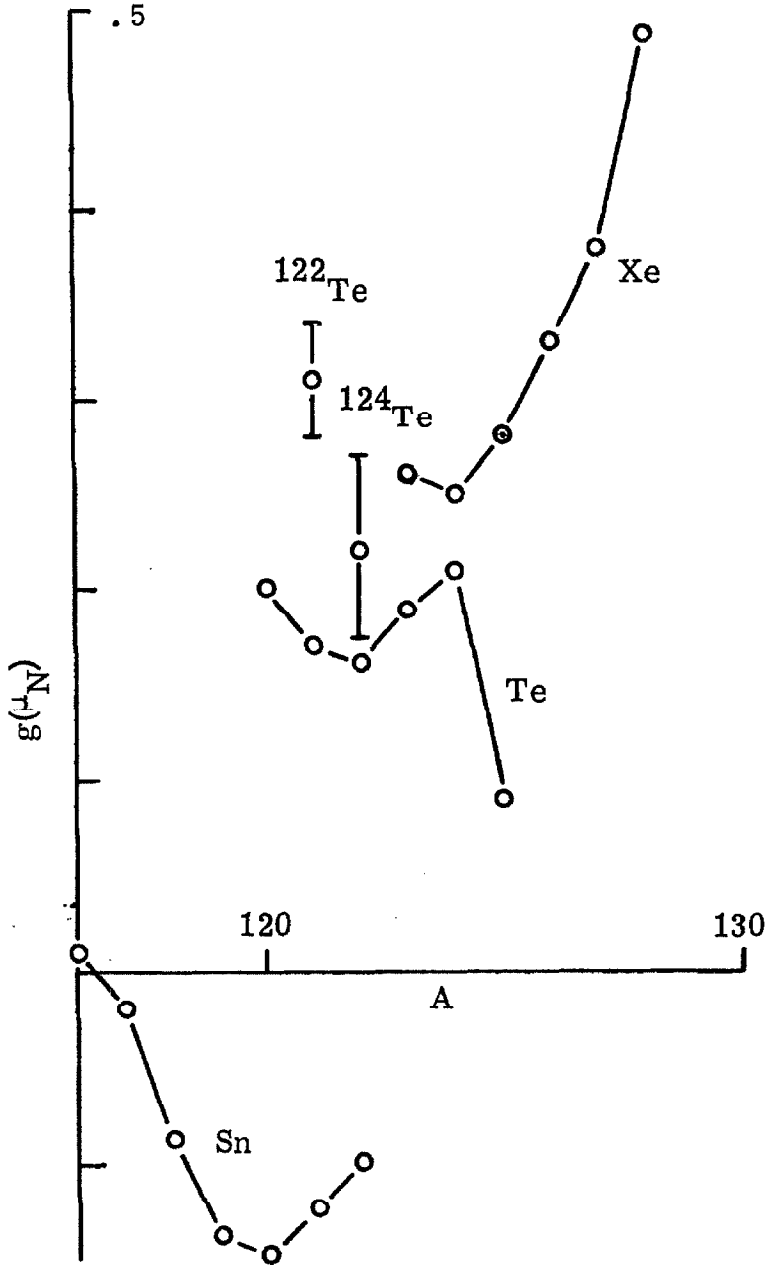

Figure 24b. Summary of the predictions of Kisslinger and Sorensen for the g factors of first excited 2^+ states in isotopes of Sn, Te, and Xe. Our results for ^{122}Te and ^{124}Te are also given.

VIII. DISCUSSION

We have applied the perturbed angular correlation technique to the measurement of g factors of excited nuclear states having lifetimes of the order of 10^{-11} seconds. This extension is made possible by the utilization of the large experimentally known hyperfine fields present at the nucleus of an impurity atom imbedded in an iron lattice.

The agreement between our results with those of the Coulomb excitation implantation technique is poor. This discrepancy may be explained by the hypothesis that the recoiling Coulomb excited nucleus experiences a field different from the static field in metallurgically prepared samples while it is stopping in the iron lattice.

Our experimental data, together with previously determined electromagnetic properties of ^{114}Cd, ^{122}Te and ^{124}Te, are in qualitative agreement with the vibrational model as modified by Tamura and Udagawa and Kisslinger and Sorensen. However, the agreement is not quantitative, and future theoretical investigation of these nuclei will be necessary before their low-lying energy levels can be completely understood.

We anticipate several extensions of this work. Measurements of the first excited 2^+ states of ^{110}Cd, ^{126}Te, and ^{126}Xe, all vibrational states, are possible with the existing apparatus.

The utilization larger NaI(Tl) crystals for our detectors, and the hyperfine field at the location of Sn nuclei in certain garnets[38], should make possible the measurement of the g factors of the first excited 2^+ states in ^{118}Sn and ^{120}Sn. The quadrupole moments of

several Sn nuclei have been determined and a strong dependence of neutron number is observed[39]. Kisslinger and Sorensen[3] predict negative g factors for these states, even though they are of a collective nature.

The availability of Ge(Li) solid state detectors, which have much better energy resolution than NaI(Tl) scintillation spectrometers, makes possible the study of excited states in nuclei having complicated decay schemes. For example, the measurement of g factors of several first and higher excited states are possible in ^{186}Os, ^{188}Os, ^{190}Os, and ^{192}Os, using the internal fields of Os in Fe. These nuclei are particularly interesting since they fall between a spherical and a deformed region.

REFERENCES

1. D. A. Shirley, Annual Review of Nuclear Science, 16, (1966) 89.

2. T. Tamura and T. Udagawa, Phys. Rev. 150 (1966) 783.

3. L. S. Kisslinger and R. A. Sorensen, Rev. Mod. Phys. 35 (1963) 853.

4. R. P. Borchers, J. D. Bronson, D. E. Murnick and L. Grodzins, Phys. Rev. Letters 17 (1966) 1099.

5. E. L. Brady and M. Deutsch, Phys. Rev. 78 (1950) 558.

6. H. Aeppli, H. Albers-Schönberg, A. S. Bishop, H. Frauenfelder and E. Heer, Phys. Rev. 84 (1951) 370.

7. K. Alder, Helv. Phys. Acta 25 (1952) 235; K. Alder, Phys. Rev. 84 (1951) 369; A. Abragam and R. V. Pound, Phys. Rev. 92 (1953) 943; R. M. Steffen and H. Frauenfelder, "The influence of extranuclear fields on angular correlations", Perturbed Angular Correlations, (North Holland, Amsterdam, 1958) p. 1.

8. B. N. Samoilov, V. V. Sklyarevskii and E. P. Stepanov, Zh. Eksp. i. Teor. Fiz. 36 (1959) 1944; 38 (1960) 359.

9. R. B. Frankel, J. Huntzicker, E. Matthias, S. S. Rosenblum, D. A. Shirley and N. J. Stone, Phys. Letters, 15 (1965) 163.

10. L. Niesen, J. Lubbers, H. Postma, H. DeWaard and S. A. Drentje, Phys. Letters, 24B (1967) 144.

11. R. E. Watson and A. J. Freeman, Phys. Rev. 123 (1961) 2027.

12. E. Matthias, E. Karlsson, A. G. Svensson, K. Johansson, and P. Da. R. Andrade "Measurements of combined magnetic and electric perturbations in polycrystalline sources", Perturbed Angular Correlations (North Holland, Amsterdam, 1964) 257.

13. M. Kontani and J. Itoh, J. Phys. Soc. Japan, 22 (1967) 345.

14. J. W. Corbett, "Electron Radiation Damage in Semiconductors and Metals", Solid State Physics (Academic Press, New York and London, 1966) Vol. 7, p. 279.

15. D. A. Shirley and G. A. Westenburger, Phys. Rev. 138 (1965) A170; R. G. Holliday, D. A. Shirley and N. J. Stone, ibid. 143 (1966) A132.

16. Nuclear Data Sheets, Nuclear Research Council, Washington.

17. ibid.

18. R. M. Steffen and H. Frauenfelder "Angular Correlations" Alpha-, Beta- and Gamma-Ray Spectroscopy, Ed. Kai Siegbahn (North Holland, Amsterdam, 1966) Vol. 2, p. 1183.

19. Nuclear Data Sheets, Nuclear Research Council, Washington; F. K. McGowan, R. L. Robinson, P. H. Stelson and J. L. C. Ford, Jr., Nuc. Phys. 66 (1965) 97.

20. P. H. Stelson and L. Grodzins, Nuclear Data, 1 (1965) 21.

21. E. Matthias, S. S. Rosenblum, D. A. Shirley, Phys. Rev. Letters, 14 (1965) 46.

22. Nuclear Data Sheets, Nuclear Research Council, Washington.

23. K. Johansson, E. Karlsson and R. W. Sommerfeldt, Phys. Letters, 22 (1966) 297.

24. K. Auerbach, B. Harms, K. Siepe, G. Wittkemper and H. J. Korner, Phys. Letters, 22 (1966) 299.

25. M. Hansen, Constitution of Binary Alloys, (McGraw-Hill, New York, 1958) p. 708.

26. G. Hägg, Nova Acta Regial Soc. Sci. Upsa liensis 4 (1929) 115.

27. W. Geller, Arch. Eisenhüttenw., 13 (1939) 263.

28. Nuclear Data Sheets, Nuclear Research Council, Washington.

29. B. Herskind, J. D. Bronson, R. R. Borchers, L. Grodzins and D. E. Murnick, Bull. Am. Phys. Soc. II 12 (1967) 503.

30. K. Auerbach, K. Siepe, J. Wittkemper and H. J. Korner, Phys. Letters 23 (1966) 367.

31. E. N. Kaufmann, private communication.

32. G. Scharff-Goldhaber and J. Weneser, Phys. Rev. 98 (1955) 212.

33. A. Bohr and B. R. Mottelson, Kgl. Danske Videuskab. Selskali, Mat. fys. Medd. 27 (1953).

34. Nuclear Data Sheets, Nuclear Research Council, Washington. F. K. McGowan, R. L. Robinson, P. H. Stelson, and J. L. C. Ford, Nuc. Phys., 66 (1965) 97. K. Johansson, E. Karlsson and R. W. Sommerfeldt, Phys. Letters 22 (1966) 297.

35. J. de Boer, R. G. Stokstad, G. D. Symons, and A. Winther, Phys. Rev. Letters 14 (1964) 564.

36. P. H. Stelson, W. T. Milner, J. L. C. Ford, Jr., F. K. McGowan, and R. L. Robinson, Bull. Am. Phys. Soc., 10 (1965) 427.

37. J. J. Simpson, D. Eccleshall, and M. J. K. Yates (to be published).

38. K. P. Belov and I. S. Lyubutin, San. Phys. J. E. T. P., 22 (1966) 578. K. P. Belov and I. S. Lynbutin, J. E. T. P. Letters, 1 (1965) 26.

39. A. M. Kleinfield, J. de Boer, Renata Conello-Moro and H. P. Lie, Bull. Am. Phys. Soc. 12 (1967) 564.